Evaluation for the Impacts of Numerical Advection Schemes and Turbulence Modeling on Gray-Zone Simulation of a Squall Line

Jianan Chen,[a] Xiaoming Shi,[a,b]

[a] *Hong Kong University of Science and Technology, Hong Kong SAR, China*

[b] *Center for Ocean Research in Hong Kong and Macau, Hong Kong University of Science and Technology, Hong Kong, China*

Corresponding author: Xiaoming Shi, shixm@ust.hk

Evaluation for the Impacts of Numerical Advection Schemes and Turbulence Modeling on Gray-Zone Simulation of a Squall Line

Jianan Chen [a] and Xiaoming Shi[a,b]

[a] *Hong Kong University of Science and Technology, Hong Kong SAR, China*

[b] *Center for Ocean Research in Hong Kong and Macau, Hong Kong University of Science and Technology, Hong Kong, China*

Corresponding author: Xiaoming Shi, shixm@ust.hk

ABSTRACT: With increasing computational power, atmospheric simulations have approached the gray zone resolutions where energetic turbulent eddies are partly resolved. The representation of turbulence in the gray zone is challenging and sensitive to the choices of turbulence models and numerical advection schemes. Some numerical advection schemes are designed with numerical dissipation to suppress small-scale numerical oscillations. However, at gray zone resolutions, the numerical dissipation can dampen both numerical and physical oscillations. In this study, we first evaluate the impact of advection schemes on the simulation of an idealized squall line at two gray zone resolutions (1 and 4 km). We found that at the 4-km resolution, the implicit numerical dissipation from advection schemes is excessive because it dampens convective cells across all scales and weakens the front-to-rear flow, producing insufficient convective precipitation and excessive stratiform precipitation. At the 1-km resolution, the numerical dissipation is desired, because without it, excessive spurious numerical oscillations develop into convections, weakening the large-scale front-to-rear flow through increased entrainment and mixing. The dynamic reconstruction model (DRM) of turbulence is designed to model both forward- and backscatter, having the potential to counter the effect of numerical dissipation from the advection schemes. Previous studies suggest superior performances of DRM in gray zone simulations for various atmospheric flows. Here, we show that although DRM can improve the squall line simulation at the 4-km resolution where the numerical damping is unwanted, it cannot improve squall line simulations at the 1-km resolution where numerical dissipation is needed.

SIGNIFICANCE STATEMENT: This work investigates the effects of numerical mixing arising from numerical advection schemes and physical mixing from turbulence schemes on an organized deep convective system in the gray zone. The numerical mixing is found to be critical in shaping the deep convective system structure and corresponding precipitation distribution. Meanwhile, the role of numerical mixing varies with gray zone resolutions. The numerical mixing is necessary when it primarily acts on spurious numerical oscillations but unfavorable when it mainly acts on physical convections. Turbulence schemes that aim to minimize numerical mixing may trigger spurious convections, which, in turn, affect the structure of the organized deep convective system via excessive entrainments.

1. Introduction

Subgrid-scale (SGS) turbulence mixing is important for convection-permitting simulations because of its vital role in transporting momentum, heat, and other scalars (Honnert et al. 2020). With increasing computational power, grid resolutions have reached the kilometer scale, which is in the gray zone for convection ((Chow et al. 2019). In the mesoscale simulations at resolutions far coarser than the kilometer scale, the subgrid turbulence mixing is parameterized using one-dimensional planetary boundary layer (PBL) schemes under the assumption that turbulence is unresolved (Chow et al. 2019; Shi et al. 2019). In large eddy simulations (LES) with grid spacing far smaller than the kilometer scale, the subgrid turbulence mixing is parameterized using three-dimensional turbulence closure models under the assumption that the energy-containing eddies are resolved (Shi et al. 2019). However, neither of those assumptions fit in the gray zone simulations where the energy-containing eddies are partly resolved. The challenge in gray zone simulations is confronted at two main directions, either through improving the PBL schemes (e.g., Shin and Hong 2015) or adapting the LES turbulence models (e.g., Parodi and Tanelli 2010). The direction of implementing LES-type closure has demonstrated superior performance compared to PBL schemes (Chow et al. 2019).

In addition to the explicit mixing due to subgrid turbulence schemes, the implicit mixing (i.e., numerical dissipation and dissipation) due to numerical advection schemes is also of significant importance in gray zone simulations (Beare 2014). Previous research suggests that numerical dissipation affects convective cells more than the explicit mixing from subgrid turbulence scheme in gray zone resolutions of squall lines simulations (Weisman et al. 1997). The numerical dissipation of advection schemes is due to the truncation errors that are formulated as a diffusive operator (Durran 2010). In numerical simulations, numerical dissipation has a critical role in damping spurious numerical oscillations that are often caused by computing the high-order approximations using the grid points near the sharp gradient (Borges et al. 2008). Sharp gradients are ubiquitous in atmospheric simulations, such as the thermodynamic processes associated with the moisture, temperature discontinuity (Wang et al. 2021).

Advection schemes are categorized as odd-order or even-order based on the type of difference approximation used for the spatial derivatives. Even-order schemes use central differencing approximations, while odd-order schemes typically use upwind approximations (Kusaka et al. 2005). Different from odd-order scheme, which has inherent numerical dissipation, even-order schemes have no numerical dissipation (Durran 2010). Without numerical dissipation, spurious numerical oscillations may develop into grid-scale convections. As a result, an even-order advection scheme typically needs an extra artificial dissipation term with coefficients that are specified empirically (Durran 2010; Xue 2000). The odd-order schemes, such as the fifth-order advection scheme (hereafter ODD5) and the fifth-order Weighted Essentially Non-Oscillatory (WENO5) scheme, are popularly used schemes in atmospheric models such as WRF (Skamarock et al. 2008) and Cloud Model 1 (Bryan and Fritsch 2002), probably because they are in the balance of computational efficiency and accuracy. In addition, there is no need to specify an extra numerical dissipation term needed in the even order scheme. Compared with ODD5, the WENO5 is often viewed as a more advanced advection scheme, which gives non-oscillatory solutions by increasing the numerical dissipation near the sharp gradient (Jiang and Shu 1996; Pressel et al. 2015). It has been shown that the increased implicit numerical dissipation of the WENO5 scheme is beneficial in dampening the grid scale erroneous convections and reducing spurious numerical oscillations (Pressel et al. 2015; Bryan 2005). The WENO schemes are also recommended in coarser resolution simulations because fewer numerical oscillations are induced (Pressel et al. 2015; Wang et al. 2021).

Nonetheless, the numerical dissipation of advection schemes is not always beneficial. For example, the numerical dissipation from the WENO scheme has been found to suppress the energy cascade in turbulence-resolving simulations and subsequently leads to unsatisfactory predictions of turbulence characteristics (Wang et al. 2021). Different from the mixing due to subgrid turbulence schemes, which are physically based, the numerical dissipation acts on small-scale motions indiscriminately (Takemi and Rotunno 2003). Not only the unphysical, spurious numerical oscillations but also physical, realistic perturbations related to the instability growth are impacted by the numerical dissipation. In the gray zone simulations where grid size is close to the scale of energy-containing eddies (Chow et al. 2019), the numerical dissipation from the advection scheme may consume energy-containing eddies. Weisman et al. (1997) have found that increased numerical dissipation smooths the convective cells in squall simulations. However, the impact of numerical dissipation from advection schemes on the overall structure of squall lines has not been evaluated in gray zone resolutions. The first aim of this study is to evaluate the impact of numerical advection schemes on gray zone simulations of squall lines. In addition, we ask how the numerical diffusion in advection schemes can affect the squall line organization and precipitation distribution.

Traditional turbulence closure models are dissipative, in which the momentum or scalar can only be transferred from larger (resolved) scales to smaller (subgrid) scales (Chow et al. 2019). This assumption is acceptable at LES resolutions where subgrid scale motions are within the inertial subrange and mostly dissipative (e.g., Honnert et al. 2020; Sun et al. 2021). In the gray zone, the subgrid-scale motions are not dissipative. By filtering the high-resolution LES to the gray zone resolutions, previous research has found a significant amount of backscatter of momentum in the gray zone simulation of squall lines (Lai and Waite 2020) and supercells (Sun et al. 2021).

Subgrid mixing models that allow backscatter have been advocated in the gray zone simulations (Chow et al. 2019). The dynamic reconstruction model (DRM) is one of such models that allows backscattering. It uses an explicit filtering and reconstruction framework to reduce numerical error from the grid discretization (Gullbrand and Chow 2003), which enhances the fidelity of the resolved field (Chow et al. 2005). Previous research has found the DRM has significantly improved the turbulent motion in neutral boundary layers (Chow et al. 2005), convective boundary layer (Simon et al. 2019), stratocumulus-capped boundary layer (Shi et al. 2018a,b), and deep tropical convection (Shi et al. 2019). The dependence on grid resolution in the gray zone simulation has been significantly reduced. In addition, the DRM can better simulate deep tropical convection in 1-km resolution simulations regarding domain-wide characteristics such as the domain-wide precipitation amount, the distribution of clouds, and vertical fluxes (Shi et al. 2019). However, the impact of DRM on organized deep convective systems has not been assessed. The second aim is to evaluate the performance of DRM in simulating the squall line.

This paper will detail the numerical model, different turbulence schemes and advection schemes in Section 2. Section 3 describes the results of the benchmark simulation. The impacts of implicit (inherently from odd-order scheme) and explicit numerical dissipation (used with even-order scheme) on squall line simulations are explored in Section 4 and Section 5 respectively. The performance of DRM is evaluated in Section 6. Section 7 summarizes and gives conclusions.

2. Method

a. Turbulence closure schemes

In large eddy simulations, turbulence closure is used to model subgrid motions. The grid mesh separates the subgrid-scale motion and the motion larger than the grid. However, due to the grid discretization and the discrete differentiation operation, only the motions larger than the model's effective resolution (larger than Δx) can be resolved (Chow et al. 2005). The turbulent motions are divided into resolved and subfilter scale (SFS). The modeling of SFS turbulence differs between closure models (Shi et al. 2018b). In this study, we mainly compare two closure models. One is a traditional LES closure, 1.5-order Turbulent Kinetic Energy (TKE) scheme (Moeng 1984; Deardorff 1980), with no backscattering allowed. The other is the DRM (Chow et al. 2005), which permits the backscatter.

1) 1.5 order TKE model

The 1.5-order TKE model is a traditional LES closure with the eddy viscosity-based form ((Deardorff 1980)). The SFS momentum flux is formulated as,

$$\tau_{ij} = -2K_m\overline{S_{ij}}, \tag{1}$$

where K_m is is the eddy viscosity and $\overline{S_{ij}}$ is the resolved turbulent strain tensor. The SFS scalar flux is similarly formulated as,

$$\tau_{ij} = -K_h\frac{\partial\overline{\theta}}{\partial x_j}, \tag{2}$$

where K_h is the eddy diffusivity and $\overline{\theta}$ represents a scalar variable. The K_h and K_m are determined by the SFS TKE (for details, see Eqs. (7) and (8) in Shi et al. (2018b)) that are predicted by a prognostic equation (Moeng 1984). The key assumption of this closure method is that the resolved turbulence generates downgradient fluxes and transfers their energy and scalar variance to smaller turbulences.

2) Dynamic Reconstruction Model

DRM is a more advanced turbulence closure model that partitions the SFS fluxes into resolvable subfilter-scale (RSFS) and subgrid-scale (SGS) components. The RSFS refers to the turbulent motion scales larger than the explicit filter but smaller than the effective resolution (Chow et al. 2005). The turbulent motions in the RSFS are partly resolved and able to produce counter-gradient fluxes in gray zone simulations (Chow et al. 2005). In the traditional LES closure, the SFS and resolved motions are divided through the implicit filter, which can differ for each term in equations, making the reconstruction of RSFS impossible (Chow et al. 2005). In contrast, the DRM defines and applies an explicit filter enabling the reconstruction of RSFS. The approximate deconvolution method is employed to reconstruct the RSFS stress (Stolz and Adams 1999). The velocity field is constructed by the following equation,

$$\tilde{u}^* = \overline{\tilde{u}_i} + (\boldsymbol{I} - \boldsymbol{G}) * \overline{\tilde{u}_i} + (\boldsymbol{I} - \boldsymbol{G}) * \left[(\boldsymbol{I} - \boldsymbol{G}) * \overline{\tilde{u}_i} \right] + \ldots, \tag{3}$$

where $\boldsymbol{G}$ is an explicit filter, $\boldsymbol{I}$ is the identity operator, the grid discretization is represented by the tilde sign, and the effect of the explicit filter is represented by the overbar sign. The reconstruction order is featured by the number of terms used on the right side of the equation. The reconstruction of the nth order maintains the initial $n+1$ terms on the right-hand side. A higher order of reconstruction allows the velocity field to be better reconstructed (Simon et al. 2019). However, the DRM shows diminishing improvement with increased order (Shi et al. 2018b). The high order of reconstruction in the gray zone involves the use of more grid cells for reconstruction and may introduce spurious mixing (Shi et al. 2018b). Here, we consider order two and order zero reconstruction, referred to as DRM0 and DRM2 hereafter. DRM2 is expected to have larger RSFS contributions than DRM0 due to the higher level of reconstruction. The SFS stress in DRM is formulated as,

$$\tau_{ij} = -2K_m\bar{S}_{ij} + \left(\overline{\tilde{u}_i^*\tilde{u}_j^*} - \overline{\tilde{u}_i^*}\,\overline{\tilde{u}_j^*}\right) \tag{4}$$

and the SFS flux is formulated as,

$$\tau_{\theta j} = -K_h\frac{\partial\bar{\theta}}{\partial x_i} + \left(\overline{\tilde{\theta}^*\tilde{u}_j^*} - \overline{\tilde{\theta}^*}\,\overline{\tilde{u}_j^*}\right) \tag{5}$$

where u and θ represent velocities and a scalar variable respectively, and the star denotes reconstructed variables. The eddy viscosity coefficient K_m is calculated using a dynamic eddy-viscosity procedure described in Chow et al. (2005) who adopted the method developed by Wong and Lilly (1994). The eddy diffusivity K_m is calculated simply by specifying a Prandtl number (Pr), $K_h = K_m/Pr$, where the Pr is 1/3.

b. Advection schemes

Considering the advection equation in the one dimension, the tendency of a variable ϕ in CM1 is computed as:

$$\frac{\partial(\phi)}{\partial t} = -\frac{\partial(U\phi)}{\partial x}, \tag{6a}$$

$$-\left.\frac{\partial(U\phi)}{\partial x}\right|_{x=x_i} = -\frac{1}{\Delta x}\left(U_{i+\frac{1}{2}}\phi_{i+\frac{1}{2}} - U_{i-\frac{1}{2}}\phi_{i-\frac{1}{2}}\right) = -\frac{1}{\Delta x}\left(F_{i+\frac{1}{2}} - F_{i-\frac{1}{2}}\right), \tag{6b}$$

where the F_i is the flux at the grid i, U is the wind speed. The Arakawa-C staggered grid (Arakawa and Lamb 1977) is the only grid system considered in this study.

1) The six-order scheme

The six-order advection scheme uses centered six-order differencing. The $\phi_{i-1/2}$ is approximated with six filtered grid values,

$$\phi^{6th}_{i-\frac{1}{2}} = \frac{1}{60}\left(\phi_{i-3} - 8\phi_{i-2} + 37\phi_{i-1} + 37\phi_i - 8\phi_{i+1} + \phi_{i+2}\right). \tag{7}$$

The centered difference scheme has no numerical dissipation, which is therefore prone to numerical instabilities and spurious numerical oscillations (Pressel et al. 2015). An additional explicit artificial dissipation term is often added to the centered advection scheme to remove the shortest waves and long waves are relatively uninfluenced (Durran 2010).

2) The fifth-order scheme

Different from the six-order scheme, the fifth-order scheme has implicit numerical dissipation. The $\phi_{i-\frac{1}{2}}$ of fifth order is computed as (Wicker and Skamarock 2002),

$$\phi^{5th}_{i-\frac{1}{2}} = \frac{1}{60}\left(2\phi_{i-3} - 13\phi_{i-2} + 47\phi_{i-1} + 27\phi_i - 3\phi_{i+1}\right). \tag{8}$$

Indeed, the $\phi_{i-\frac{1}{2}}$ of the fifth order is equivalent to the sum of $\phi_{i-\frac{1}{2}}$of sixth order and a six-order dissipation term (Wicker and Skamarock 2002):

$$\phi^{5th}_{i-\frac{1}{2}} = \phi^{6th}_{i-\frac{1}{2}} + \frac{1}{60}\left(\phi_{i-3} - 5\phi_{i-2} + 10\phi_{i-1} - 10\phi_i + 5\phi_{i+1} - \phi_{i+2}\right). \tag{9}$$

3) The fifth-order WENO scheme

The fifth-order WENO scheme improves the fifth-order advection scheme near the sharp gradient (Jiang and Shu 1996). It can achieve non-oscillatory near the sharp gradient. In the fifth-order scheme, the five grid points can be separated into three stencils. The $\phi_{i-\frac{1}{2}}$ can approximated by each stencil S (Jiang and Shu 1996),

$$\phi^{(S=0)}_{i-\frac{1}{2}} = \frac{1}{6}\left(2\phi_{i-3} - 7\phi_{i-2} - \phi_{i-1}\right), \tag{10a}$$

$$\phi^{(S=1)}_{i-\frac{1}{2}} = \frac{1}{6}\left(-\phi_{i-2} + 5\phi_{i-1} + 2\phi_i\right), \tag{10b}$$

$$\phi^{(S=2)}_{i-\frac{1}{2}} = \frac{1}{6}\left(2\phi_{i-1} + 5\phi_i - \phi_{i+1}\right). \tag{10c}$$

The linear combination of the three stencils gives the fifth-order approximation,

$$\phi_{i-\frac{1}{2}} = w_0\phi^{(S=0)}_{i-\frac{1}{2}} + w_1\phi^{(S=1)}_{i-\frac{1}{2}} + w_2\phi^{(S=2)}_{i-\frac{1}{2}}, \tag{11}$$

which is the same as Eq. 8 when $w_0 = 1/10$, $w_1 = 3/5$, and $w_2 = 1/10$. The WENO scheme maintains fifth-order accuracy in the smooth region and non-oscillatory near the sharp gradient by assigning nonlinear weights to each stencil based on a smoothness indicator (Jiang and Shu 1996). When a stencil encounters a sharp gradient, the stencil will be assigned to a smaller weight. This weighting strategy leads to a smoothing effect near the sharp gradient and can suppress the generation of numerical oscillations. CM1 applies an improved version called WENO-Z (Borges et al. 2008). The details of the smoothness indicator are documented in Borges et al. (2008).

c. Numerical models and setup

The model used is the Cloud Model 1, a state-of-the-art atmospheric model that can solve the non-hydrostatic, compressible equations of the moist atmosphere (Bryan and Fritsch 2002). In this study, we use three different horizontal grid spacings: 200 m, 1 km, and 4 km. The domain dimension is 96 km (Y) $\times$ 640 km (X) $\times$ 25km (Z) for 200-m and 1-km resolution simulations. For the squall line simulations, the 200-m grid resolution is typically within the LES resolutions where the inertial subrange can be resolved (Bryan and Morrison 2012; Bryan et al. 2003; Lai and Waite 2020). The 1 and 4 km grid spaces are within the gray zone resolutions of the squall line simulation. The mesoscale structures of squall lines are resolved in the 1 km and 4 km simulations, but the energy peak is not resolved, and substantial subgrid turbulence kinetic energy exists in these resolutions (Weisman et al. 1997; Bryan et al. 2003). For the 4-km resolution simulations, we enlarge the domain with the size of 240 km (Y) $\times$ 640 km (X) $\times$ 25 km (Z). Domains of all simulations in this study are not translated. A Rayleigh damper is applied at vertical levels above 20 km. The vertical grid size for 1 km and 4 km simulations stretches from 100 m at low levels to 500 m at high levels. For 200 m simulations, the grid size stretches from 50 m at low levels to 100 m at high levels. The results presented in this study are not sensitive to the vertical grid spacings. A periodic boundary condition is used in the Y direction, while an open boundary is used in the X direction. The microphysics scheme is the Morrison scheme (Morrison et al. 2009).

The model is integrated up to 6 hours when the squall-line cold outflow boundary is still within the computational domain. Following Lai and Waite (2020), the input wind profile (Fig. 1) is based on a classic weak shear case (Weisman and Rotunno 2004) but subtracting a mean wind speed of 10 m/s from the original weak shear wind profile. This is to ensure that the simulated squall lines are far away from the open boundary during the simulation period. The other sounding profiles are the same as the profiles used in Weisman and Rotunno (2004). The squall line is initiated using a

2-km-deep cold pool where the maximum potential temperature perturbation is set at the surface with -8 K. The initiated cold pool is infinite in the Y direction and extends 80 km from the left boundary (in the X direction). Random temperature perturbations are added to the lowest levels to allow the generation of three-dimensional perturbations along the squall line. In the simulations, after the model's spin-up, the domain-wide rain rate of the simulations gradually levels off. The last two hours are viewed as a steady-state period and used for steady-state analysis.

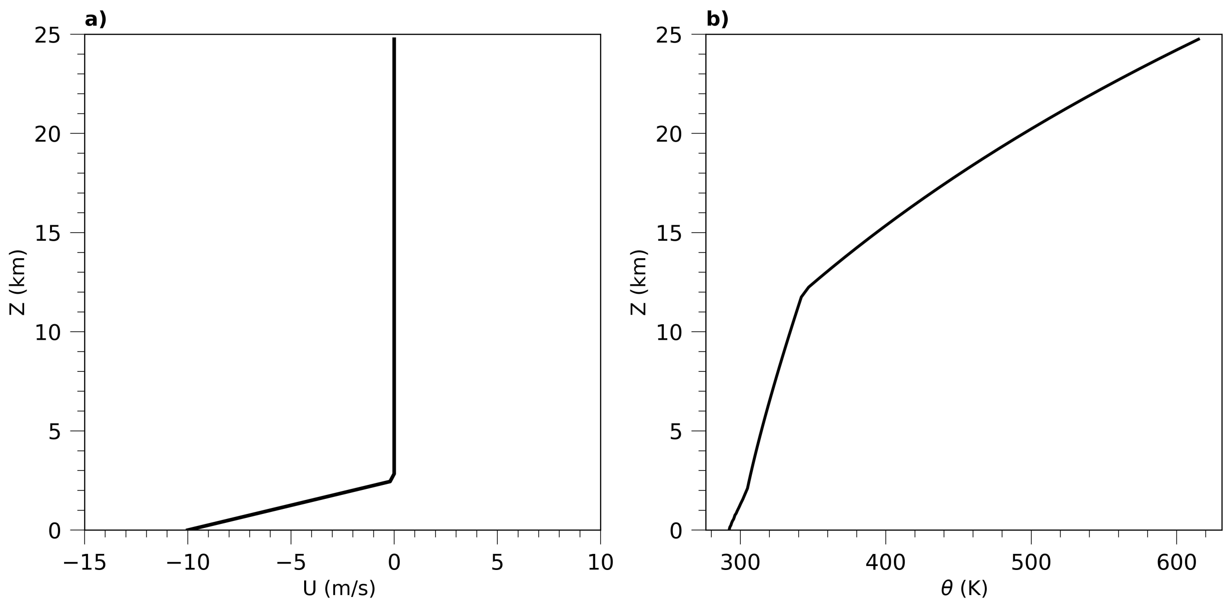

FIG. 1. Vertical profile of U and θ.

Numerical dissipation comes from both temporal and spatial grid discretization. For the time integration, all simulations use the same split-explicit Runge-Kutta scheme (Wicker and Skamarock 2002). For the spatial discretization, the simple fifth-order scheme (ODD5), fifth-order WENO scheme (WENO5), and centered sixth-order scheme (EVEN6) are used. This study adds no explicit dissipation for WENO5 and ODD5 because of implicit numerical dissipation in the schemes themselves. The vertical and horizontal directions are applied with the same advection scheme for each experiment. For the WENO5, it is applied to both scalar and momentum advection.

In CM1, the six-order explicit artificial dissipation is applied with the EVEN6 scheme. The corresponding equation is formulated as, $\partial\phi/\partial t = S + \alpha\nabla^6\phi$, where the α is the dissipation coefficient and S represents tendency due to the other terms including advection. The α is further determined by a dissipation parameter β, $\alpha = 2^{-6}\Delta t^{-1} p^{-1}\beta$, where Δt represents the time step and

Experiment Name	Advection Scheme	SGS Model	Grid Spacing Δx	Dissipation Parameter β
WENO5+TKE	Fifth-Order WENO	TKE-1.5	0.2, 1, 4 km	N/A
ODD5+TKE	Fifth-Order	TKE-1.5	0.2, 1, 4 km	N/A
EVEN6(β)+TKE	Six-Order	TKE-1.5	0.2, 1, 4 km	0, 0.02 - 0.24
WENO5+DRM0	Fifth-Order WENO	Zero Order DRM	1, 4 km	N/A
WENO5+DRM2	Fifth-Order WENO	Second Order DRM	1, 4 km	N/A
ODD5+DRM0	Fifth-Order	Zero Order DRM	1, 4 km	N/A
ODD5+DRM2	Fifth-Order	Second Order DRM	1, 4 km	N/A

TABLE 1. The numerical simulations conducted in this study. The name EVEN6(β)+TKE suggests the six-order advection scheme with an artificial dissipation parameter β, and TKE-1.5 as the subgrid turbulence model. Other names follow the same format.

p represents the number of passes of the diffusion scheme (Knievel et al. 2007). The recommended dissipation parameter β for six-order dissipation ranges from 0.02 to 0.24. We also consider $\beta = 0$ case, in which no explicit dissipation is applied. In addition, this study uses a simple flux-limited monotonic diffusion scheme (Xue 2000).

The numerical simulations conducted in this study are listed in Table 1. Firstly, we evaluate the impact of implicit numerical dissipation in the WENO5 and ODD5 on the squall line simulation. Secondly, the impact of numerical dissipation on the squall line structure is further investigated using EVEN6 with various degrees of artificial dissipation. Lastly, the DRMs, in replacement of TKE, are evaluated with different advection schemes.

3. Benchmark Simulation

In squall line simulations, the 200-m grid size falls within the LES resolutions. In this study, the 200-m resolution simulation using the WENO5 advection scheme and TKE turbulence scheme is employed as the benchmark simulation. The squall line at the end of the simulation (at the 6th hour) using the WENO5 is shown in Fig. 2a. Consistent with previous studies (e.g., Rotunno et al. 1988), the simulation captures the upshear-tilted squall line structure characterized by the upshear-tilted convective clouds and well-developed anvil clouds. The steady-state precipitation distribution in the cross-squall line direction is shown in Fig. 3. The leading edge of the cold pool is normalized to the same location before averaging over the steady-state period. The benchmark simulation (black solid line in Fig. 3a) shows strong convective precipitation reaching around 49 mm/ hour but very weak precipitation in the stratiform region. The peak of the precipitation is located at 24.6 km behind the gust front. The 200-m resolution simulations are less sensitive to the numerical advection schemes used. The 200-m ODD5+TKE, 200-m EVEN6(0.04)+TKE and our 200-m WENO5+TKE benchmark simulations show converged signs including similar squall line structure (2b, d, f) and steady-state precipitation distribution (Fig. 3). In addition, the simulated squall lines propagate to nearly the same location at the end of the simulation (Figs. 2), suggesting similar moving speeds. The 200-m simulations are also not sensitive to the turbulence schemes used (figures not shown).

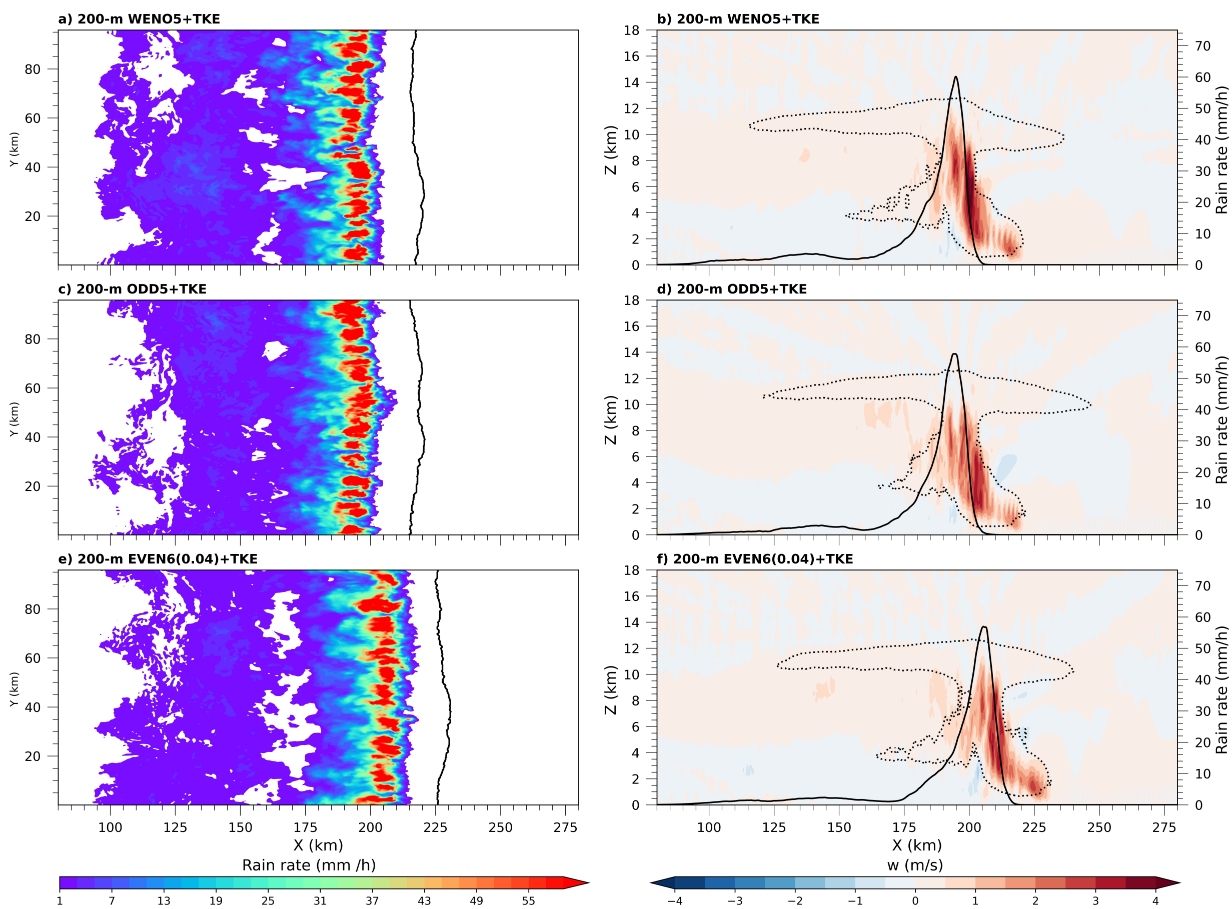

Fig. 2. Instantaneous fields (at 6th hour) of 200-m resolution simulations using WENO5 (a, b), ODD5 (c, d), and EVEN6(0.04) (e, f). The (a), (c), and (e) shows instantaneous rain rate (mm/ hour) (shaded) and cold pool location (black solid line). The (b), (d), and (f) show the line-averaged (y) vertical velocity w (m/s) (shaded), cloud boundaries (black dotted contour lines of 1×10^{-4} mixing ratio of cloud water and ice q_i+q_c), the instantaneous precipitation distribution (black solid lines, with the axis on the right). All simulations use TKE as the turbulence model.

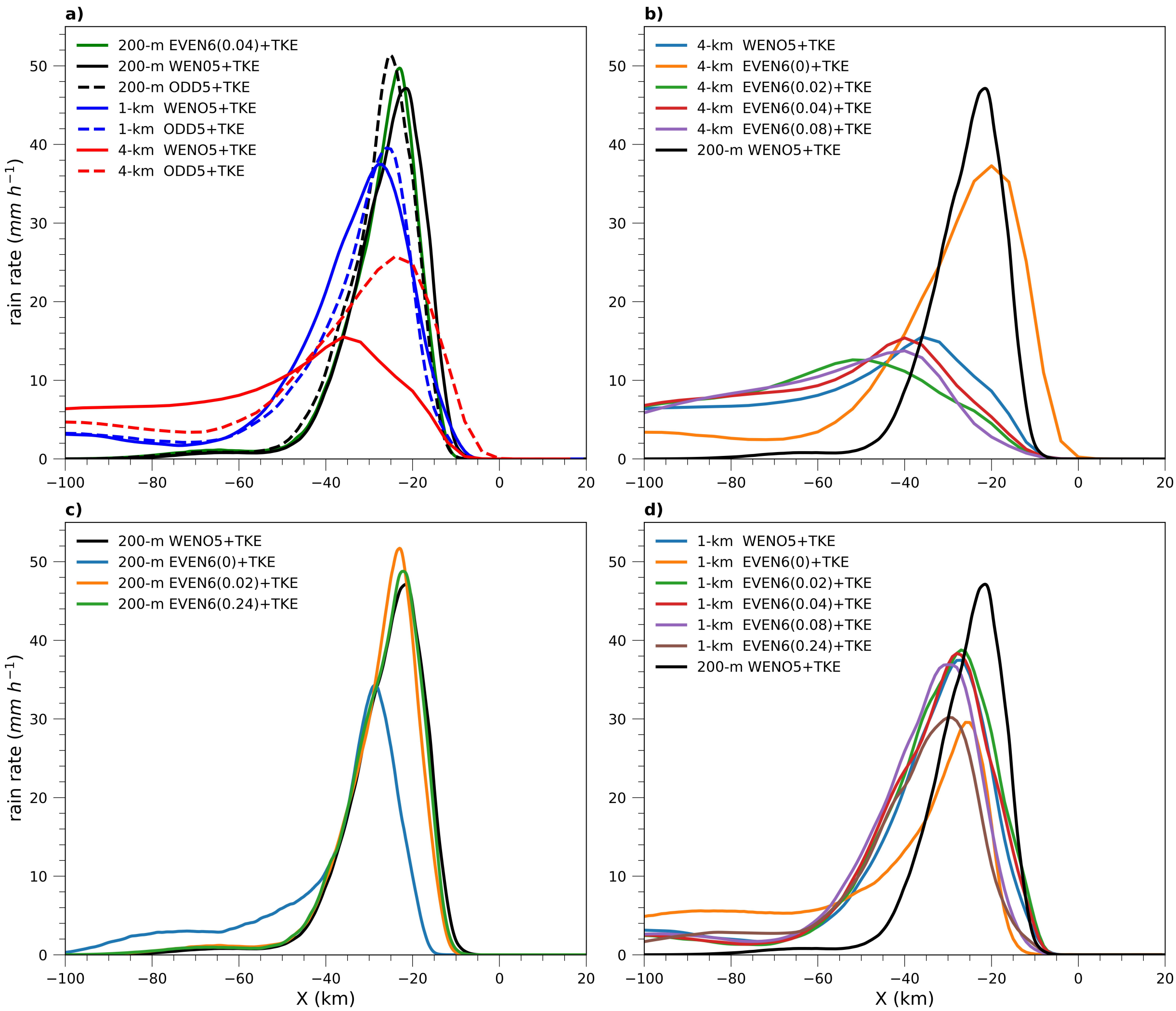

FIG. 3. The line-averaged (y) squall line steady-state rain rate distribution. The leading edge of the cold pool is normalized to the same location before averaging over the steady-state period. The leading edge of the cold pool is at 0 km. a) Simulations with resolution Δx = 200 m, 1 km, 4 km, using WENO5 (solid lines) and ODD5 (dashed lines) as the advection schemes. b) 4-km resolution simulations, and the EVEN6 as advection scheme with the artificial dissipation parameter β = 0, 0.02, 0.04, and 0.08. c) 200-m resolution simulations, and the EVEN6 as advection scheme with β = 0, 0.02, and 0.24. d) Simulations with resolution 200 m, and the EVEN6 as advection scheme with β = 0, 0.02, 0.04, 0.08, and 0.24. All simulations use TKE as the turbulence model.

4. Impact of Implicit dissipation

The ODD5 and WENO5 are popular advection schemes in which the numerical dissipation is implicit. In the 200-m LES resolution simulations, the simulated squall lines are less sensitive to the two schemes. In this section, we evaluate the impact of the two advection schemes on squall line simulations at two gray zone resolutions, 1 km and 4 km. The turbulence model employed in this section is the TKE scheme.

In the 1-km resolution, the ODD5 simulation shows a similar squall line structure (Fig. 4) and precipitation distribution (Fig. 3a) with the WENO5 simulation. However, in the 4-km resolution, the ODD5 simulation shows significantly stronger convective precipitation and weaker stratiform precipitation than the WENO5 simulation (Figs. 3a, 4). In addition, the 4-km ODD5 simulation shows much stronger vertical velocities than the 4-km WENO5 simulation (Figs. 4d, h and supplementary Fig. S1). Different from WENO5, where the numerical dissipation is enhanced near the sharp gradient to ensure non-oscillatory solutions, ODD5 has lower numerical dissipation near the sharp gradient. These results suggest that 1) the enhanced numerical dissipation near sharp gradients can affect convective updrafts, squall line structures, and the precipitation distribution, and 2) the impact of numerical dissipation on squall lines simulation intensifies with grid size.

The strength of convective updrafts in the leading edge of cold pools indeed modulates the squall line structure and the corresponding precipitation distribution. Comparing the 4-km WENO5 simulation with the 200m WENO5 benchmark simulation, the 4-km WENO5 simulation simulates trailing stratiform clouds that are more concentrated at lower levels(Figs 2a, 4d), This is because the vertical motions in the 4-km simulation are much weaker leading to a weaker ascending front-to-rear flow. This weaker ascending front-to-rear flow is not strong enough to bring lower-level moisture to reach high levels and condenses a greater portion of water at much lower heights. Therefore, the trailing stratiform cloud is developed at relatively low levels. Since the precipitation particles would fall from much lower heights, the decreased exposure time for evaporation increases the precipitation particles reaching the surface and, therefore, increases precipitation in the trailing stratiform region. Correspondingly, the precipitation distribution of the 4-km WENO5 simulation shows much weaker convective precipitation but stronger stratiform precipitation (Fig. 3a). Meanwhile, the precipitation peak for 4-km WENO5 simulation is shifted to a location far (35 km) behind the gust front.

The precipitation distribution of 1-km WENO5 (ODD5) simulation is in an intermediary position between 200-m and 4-km WENO5 (ODD5) simulation. This is because the convective updrafts weaken with grid resolutions (supplementary Fig. S1). Bryan (2012) found convective activities exhibit the greatest intensity at the 1-km resolution, surpassing both the 250-m and 4-km grid resolutions. This inconsistency is probably caused by the different initial sounding profiles used, as argued by Lai and Waite (2020). Of note, previous discussions attribute the stronger convective activities in 1-km resolution when compared with 4-km resolution to the enhancement of non-hydrostatic processes (Weisman et al. 1997; Bryan 2012). In this study, we show that the increased numerical dissipation also contributes to this weakening through numerical dampening of physical convective updrafts.

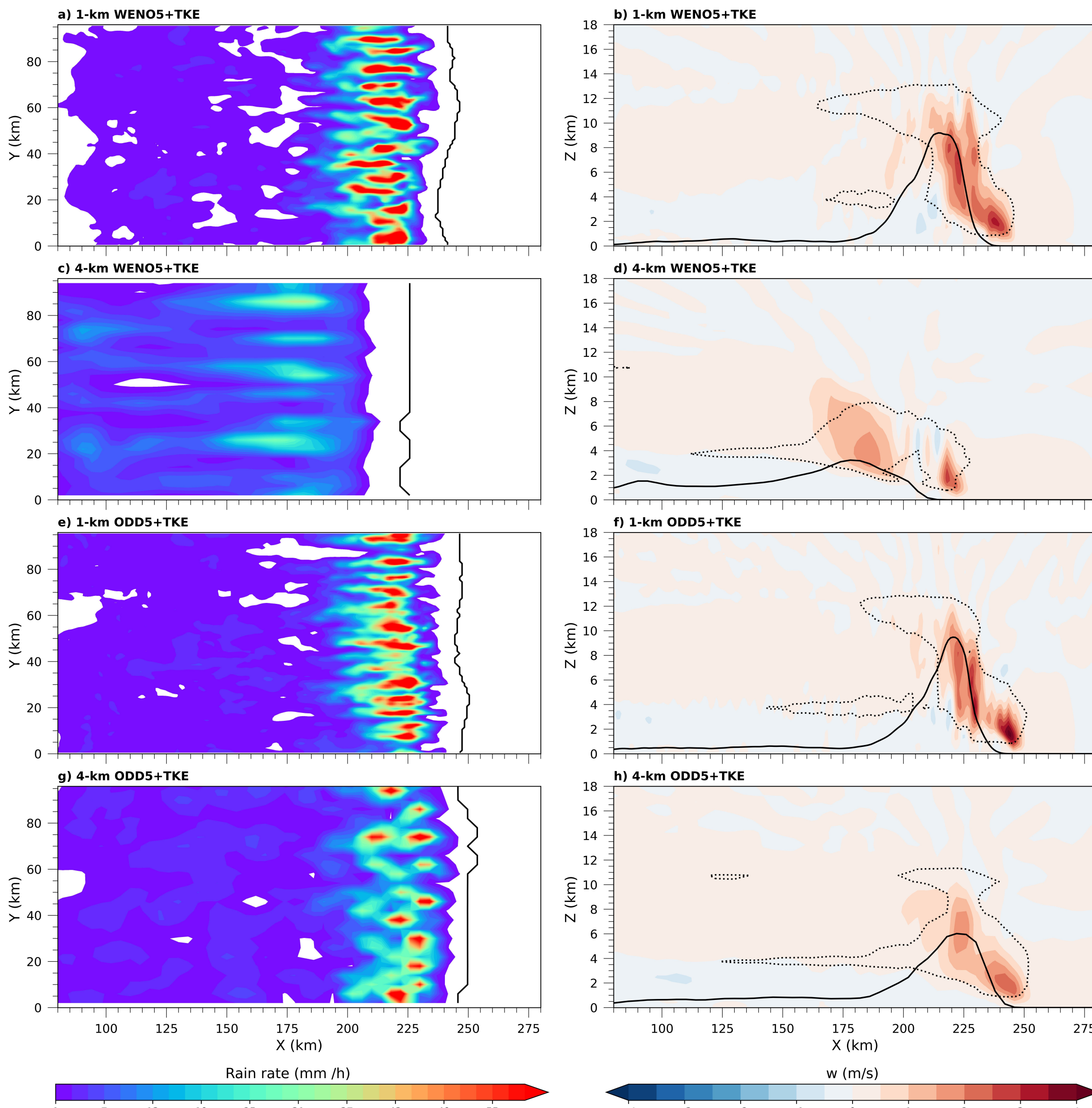

FIG. 4. Same as Fig. 2, except shows instantaneous fields (at 6th hour) of simulations 1-km WENO5+TKE (a, b), 4-km WENO5+TKE (c, d), 1-km ODD5+TKE (e, f), 4-km ODD5+TKE (g, h).

5. Impact of Explicit Dissipation

The comparison of the WENO5 and ODD5 scheme suggests that the degree of numerical dissipation can significantly impact the simulated squall line structure and corresponding precipitation distribution at the resolution of 4 km, but not at the 1 km and 200 m resolutions. It is therefore important to evaluate the impact of numerical dissipation on the squall line at different resolutions. However, the numerical dissipation in WENO5 and ODD5 is implicit and hard to quantify. In this section, the centered scheme (EVEN6) in which the numerical dissipation can be controlled by varying explicit artificial dissipation is employed. Here, we will show simulation results in the order of 4 km, 200 m, and 1 km resolution.

a. 4-km resolution simulations

The simulation results of EVEN6 scheme with artificial dissipation parameter $\beta = 0, 0.02, 0.04, 0.08, 0.24$ are shown in Fig. 5. Consistent with previous studies (Weisman et al. 1997), the convective cell size increases with the degree of numerical dissipation (Fig. 5). In addition, the increasing artificial numerical dissipation increasingly slows the squall line development (Fig. 5). For the $\beta = 0.24$ case, the squall line is too slow to evolve into the steady state (Fig. 5e, j). We exclude the $\beta = 0.24$ case in the following analysis. The numerical dissipation also impacts the overall squall line structure. Similar to the WENO5, the EVEN6 schemes with non-zero explicit dissipation show relatively low stratiform clouds, weak precipitation in the convective region, and stronger precipitation in the stratiform region (Figs. 4d and 5g, h, i). In contrast, for the $\beta = 0$ (hereafter, no-dissipation) case, the squall line has shown significantly stronger precipitation near the convective region and weak precipitation in the trailing stratiform region (Fig. 3b). The dynamics of the convective region are closely tied to the trailing stratiform region. In the no-dissipation case, the updrafts are much stronger than other schemes with implicit (ODD5 and WENO5) or explicit dissipation, further modulating the precipitation in the convective and stratiform regions. For the convective region, the stronger velocities enable deep convective clouds to form and create strong precipitation in the convective region. For the stratiform region, the stronger vertical velocities of convective updrafts enable the trailing stratiform cloud to form at higher levels. Therefore, the precipitation in the stratiform region is greatly reduced.

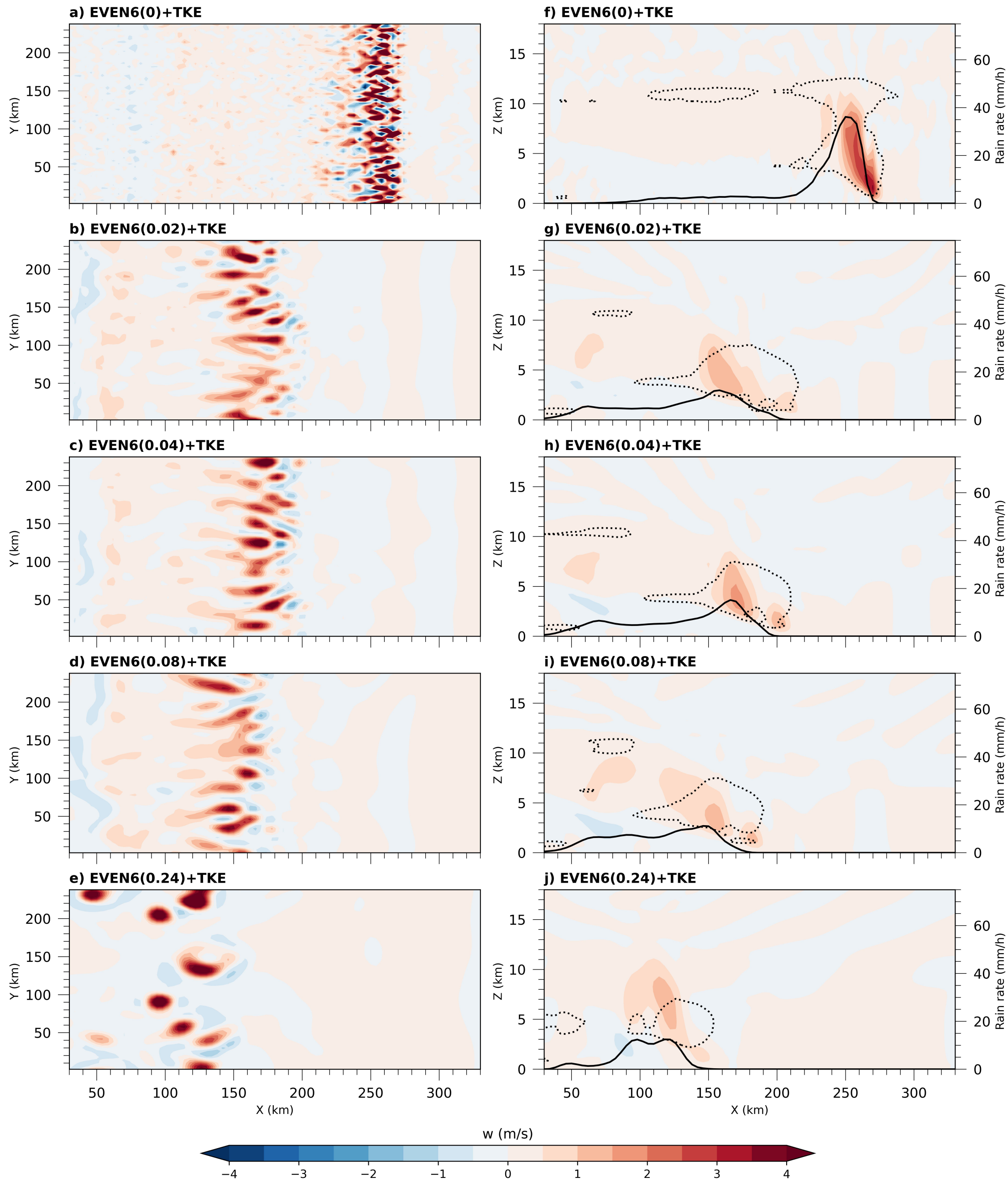

FIG. 5. The 4-km simulations using EVEN6 advection schemes with artificial dissipation parameter $\beta = 0$ (a, f), 0.02 (b, g), 0.04 (c, h), 0.24 (d, i), 0.24 (e, j). All simulations use TKE as the turbulence model. The (a), (b), (c), (d), and (e) show the horizontal slice of vertical velocity at 5 km height. The (f), (g), (h), (i), and (j) show the line-averaged (Y) averaged instantaneous fields. The 1×10^{-4} mixing ratio of cloud water and ice (q_i+q_c) black dotted contour lines show the cloud boundaries. The black solid line shows the mean precipitation distribution along the squall line with the axis on the right. The shading shows line-averaged vertical velocities w (m/s).

The effects of numerical dissipation from the advection scheme are further illustrated by the vertical velocity spectra (Fig. 6a). The computation of the spectra follows methods used in Bryan (2005). According to Skamarock (2004), the optimal spectrum at a coarse resolution would correspond to the high-resolution spectra up to the Nyquist limit of the grid. The 200-m resolution WENO5 simulation spectrum is used as the benchmark spectrum. In the along-squall-line direction, the no-dissipation case has shown slightly enhanced turbulent energy than the benchmark (Fig. 6a). Other simulations using advection schemes that have implicit or explicit numerical dissipation show weaker energy across all scales. In the cross-squall-line direction, the no-dissipation case shows even better agreement with the benchmark spectrum, except for slight energy build-up at scales close to the Nyquist limit of 8 km (Supplementary Fig. S2). Similarly, the energy is weaker across all scales in the schemes with numerical dissipation.

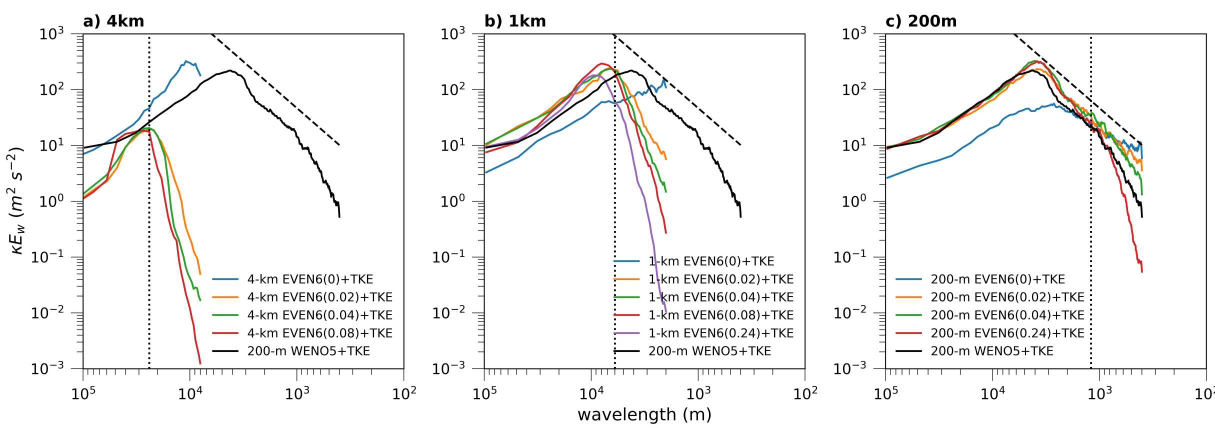

FIG. 6. One-dimensional vertical velocity (along squall line direction, at 5 km above the surface) spectra of simulations with grid resolutions of (a) 4-km, (b) 1-km, and (c) 200-m. The simulations use the EVEN6 schemes with varying artificial dissipation parameters β. The spectrum of the 200-m WENO+TKE benchmark simulation is plotted for reference. The black dashed line indicates a $k^{-\frac{5}{3}}$ spectrum. The vertical black dotted line indicates the empirical numerical dissipation scale (λ_d)

The numerical dissipation from the advection scheme cannot differentiate between the physical modes and computational noise. Small-scale perturbations are indiscriminately dampened. In the 4-km simulations, the numerical dissipation dampens physical convective cells significantly and further affects the squall line structure. In contrast, the no-dissipation case is arguably better in simulating strong convective precipitation, high-level trailing stratiform clouds, and weak precipitation in the stratiform region, because little dampening is imposed on the convective updrafts. Of note, undamped numerical oscillations may also contribute to stronger convective activity in no-dissipation simulations. It is difficult to quantify the individual contributions to the stronger convection. However, we believe that the contribution from undamped numerical oscillations is small because little grid-scale convections is visually observed in the simulation field (Fig. 5a). The presence of some spurious numerical oscillations is expected due to the smoothing of sharp gradients with a fairly coarse grid.

b. 200-m resolution simulations

The simulation results of EVEN6 scheme with artificial dissipation parameter $\beta = 0.02, 0.24$ are shown in Fig. 7. The impact of the explicit numerical dissipation decreases with increasing grid resolution. This is consistent with the speculation brought by Bryan et al. (2006) that the impact of numerical dissipation should decrease with the increasing resolution because the dissipation will not act directly on the scale of convective cells at high-resolution simulations. The dominant scale of convective cells can be indicated by the wavelength of the energy spectrum peak λ_p (Fig. 6). The empirical numerical dissipation scale (λ_d) for sixth-order dissipation is $6\Delta x$ (Durran 2010). The λ_p in the along-squall-line direction is 4 km which is larger than the dissipation scale λ_d of 1.2 km indicated by the vertical black line in Fig. 6c. Therefore, the numerical dissipation from the advection scheme can hardly dampen the dominant convective cells.

In the 200-m resolution simulations, numerical dissipation is necessary. Without the explicitly added numerical dissipation, significant spurious numerical induced convections are generated (Fig. 7a). Different from the 4 km simulations, the no-dissipation case in the 200-m simulation shows trailing clouds concentrated at low height levels, underestimated precipitation in the convective region and overestimated precipitation in the trailing region (Figs. 3c, 7d). Previous studies (e.g., Bryan 2005; Takemi and Rotunno 2003) find the spurious numerical oscillations can lead to spurious unphysical updraft patterns in the squall line simulations. The presence of moist absolutely unstable layers in the squall line environment amplifies the numerical oscillations and leads to spurious updrafts (Bryan 2005). However, the spurious updrafts are much less than the no-dissipation case presented here because the advection schemes used in their studies have implicit or explicit dissipation. To our knowledge, the impact of numerical oscillations on the general characteristics of squall lines has not been investigated.

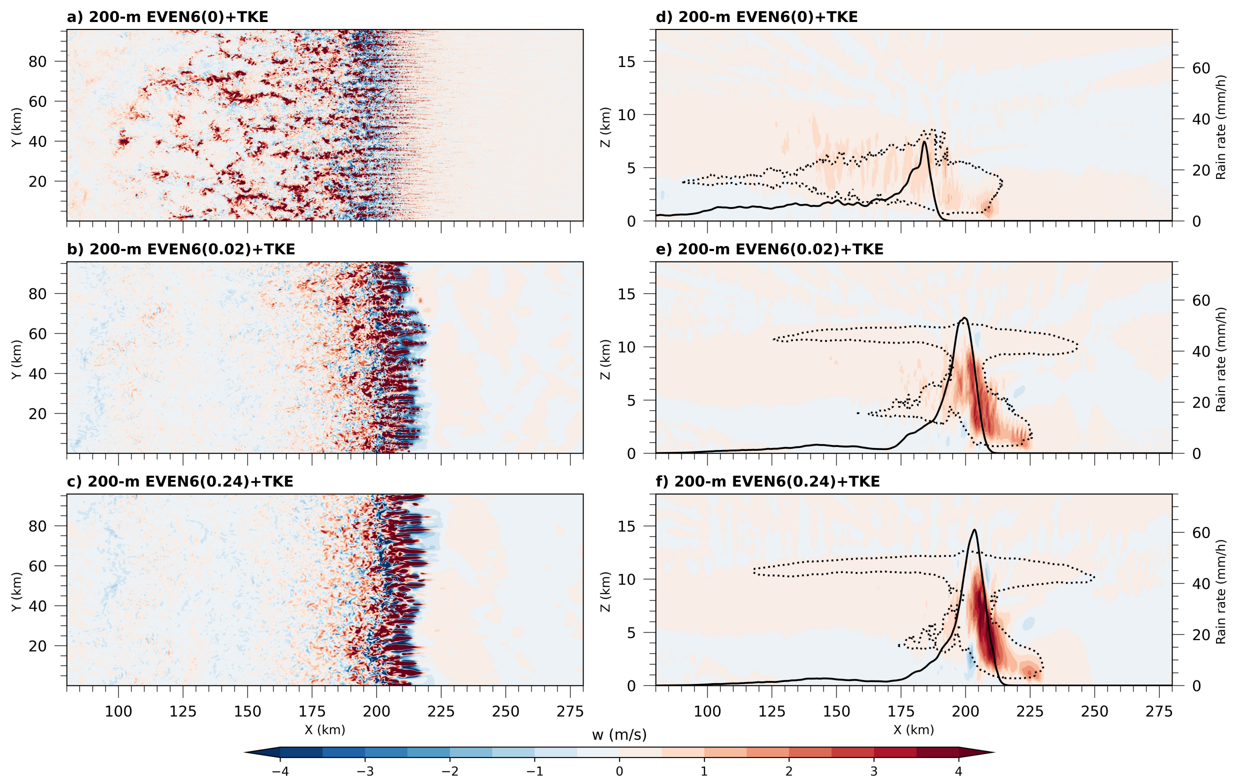

FIG. 7. Same as Fig. 5 except shows the 200 m simulations using EVEN6 advection schemes with the artificial dissipation parameter β =(a, d), 0.02 (b, e), 0.24 (c, f)

Here, we show that very spurious numerical oscillations can weaken convective updrafts through increased entrainment and subsequently affect the squall line structure. To investigate the impact of numerical oscillations, passive tracers with a mixing ratio of 1 kg/kg are included and released at the lowest 3 km. For simplicity, we compare EVEN6(0.02)+TKE with the no-dissipation EVEN6(0)+TKE simulation. The mean tracer mixing ratio in the cross-squall-line direction is shown in Fig. 8. Both simulations show a maximum tracer mixing ratio near the tropopause. This is because the tracers are transported from low to higher levels by convective updrafts but are forced to accumulate near the cloud top by the strong atmospheric stability.

At the 4-5 km height levels, the no-dissipation simulation shows higher mean tracer mixing ratios, compared with the EVEN6(0.02) scheme (Fig. 8). However, the frequencies of high tracer mixing ratios ($q_t > 0.8$ kg/kg) for all positive vertical velocities are much smaller in the no-dissipation simulation (Figs. 9a, b). This suggests more diluted convective cores in the no-dissipation simulation at the heights of 4-5 km. The marginal plots in the top and right of Fig. 9 show

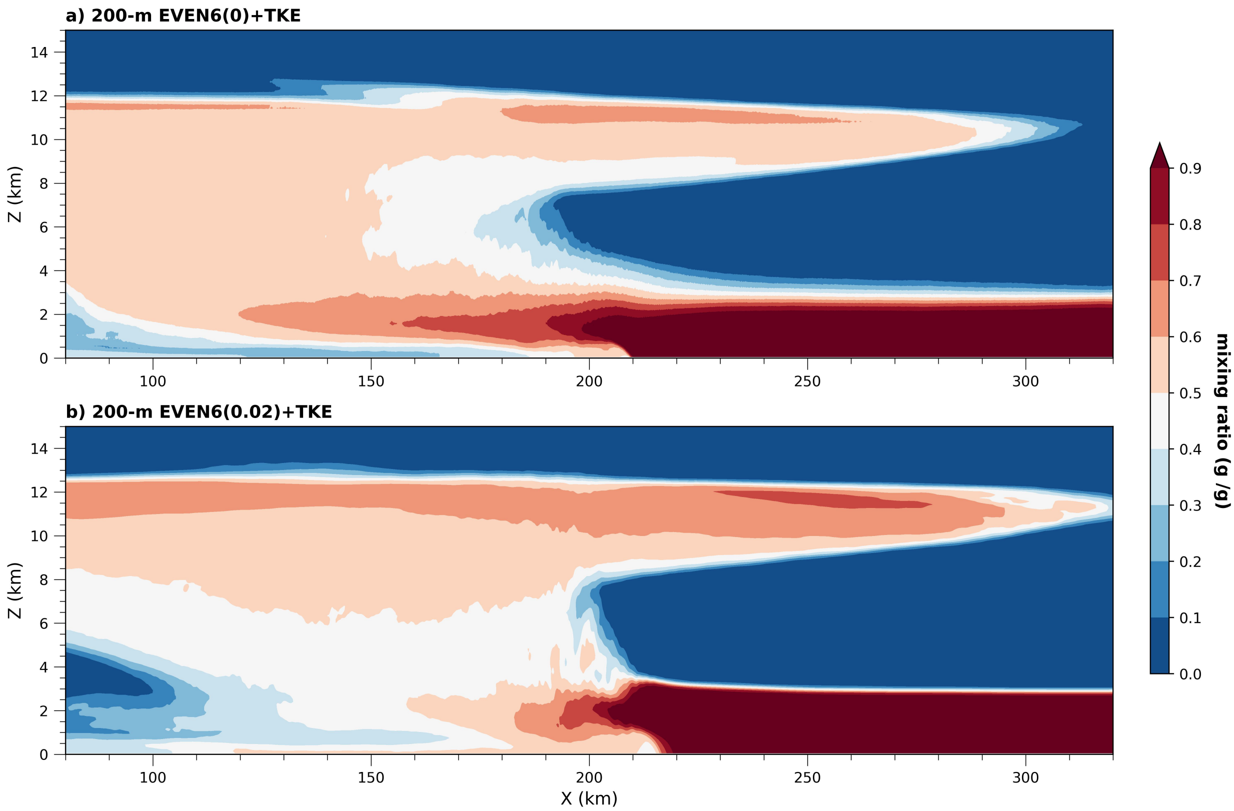

FIG. 8. Line-averaged (y) averaged passive tracer mixing ratio for simulations of a) 200-m EVEN6(0)+TKE and b) 200-m EVEN6(0.02)+TKE

the probability distribution of vertical velocities w and tracer mixing ratios q_t respectively. The no-dissipation simulation also has higher frequencies of w between 1- 6 m/s, but lower frequencies of w above 6 m/s, indicating the convective activities are more sporadic and disorganized without sufficient numerical dissipation.

At the 8-9 km height levels, compared with the EVEN6(0.02), the no-dissipation simulation shows a lower mean q_t (Fig. 8). The probability of $w > 2$ m/s is lower in the no-dissipation simulation, suggesting that the sporadic convective updrafts are less likely to reach the 8-9 km height levels. Correspondingly, the joint probability of w and q_t are more compactly distributed (Figs. 9c, d). Although the tracer concentration is higher in the no-dissipation simulation at 4-5 km heights, the tracer cannot be effectively transported upward by the sporadic convective updraft. Therefore, the tracer's concentration is higher in EVEN6(0.02) at 8-9 km heights.

In the no-dissipation simulation, the sporadic nature of numerical errors leads to the sporadic distribution of numerical oscillations. In the unstable environment, the numerical oscillations

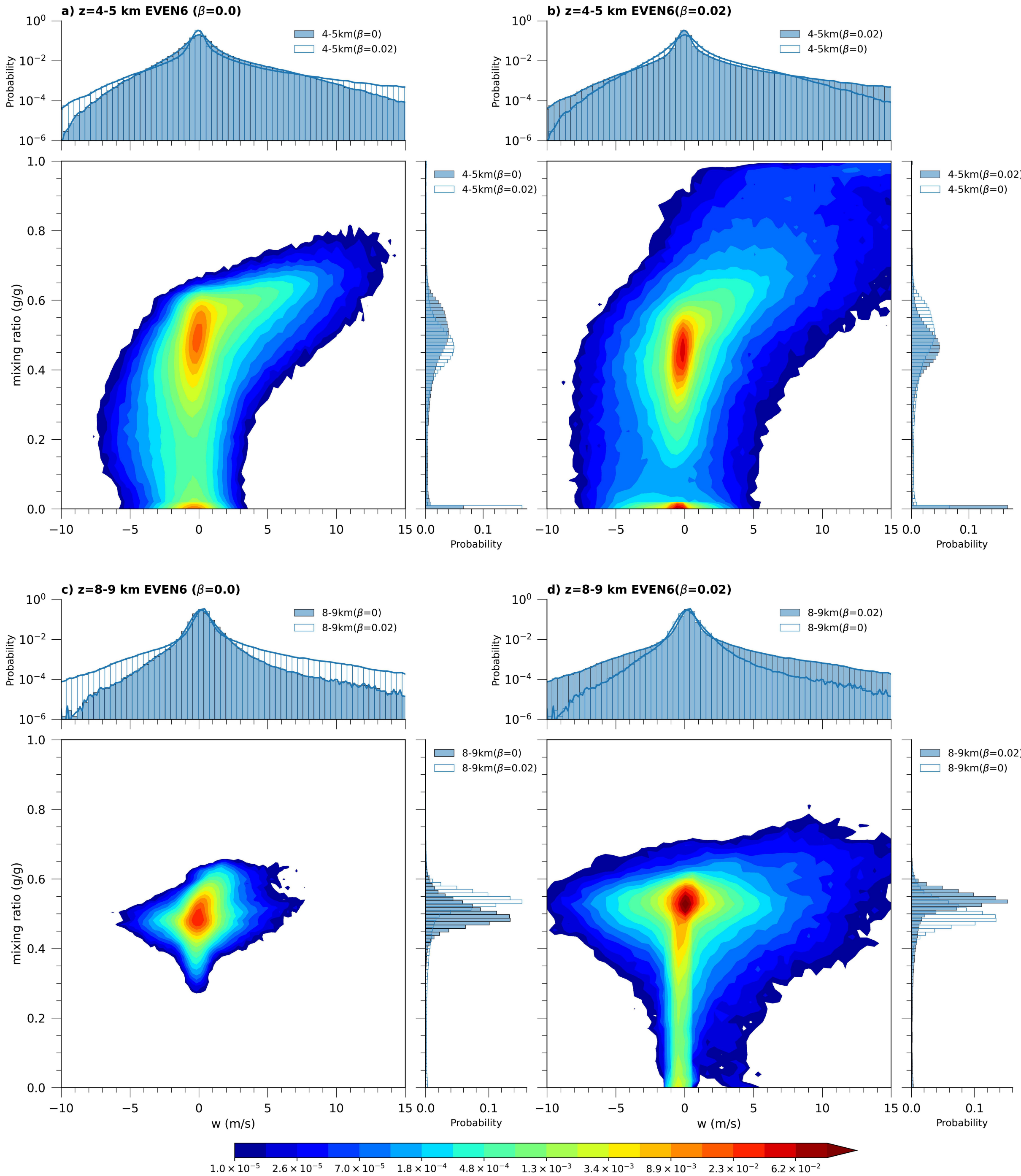

FIG. 9. The joint probability distribution of tracer mixing ratio and vertical velocities at heights of 4-5 km (a, b) and 8-9 km (c, d). (a) and (c) show the simulation of 200-m EVEN6(0)+TKE (b) and (d) show the simulation of 200-m EVEN6(0.02)+TKE. Horizontally, only data between the leading edge of the cold pool and 100 km behind the leading edge are used. The marginal plots on the upper and right show the probability distribution of vertical velocities and tracer mixing ratios respectively.

amplify and then develop into artificial numerical convections. The sporadic artificial convections increase the entrainment and mixing at low levels, leading to disorganized and weak convective updrafts. Subsequently, the front-to-rear flow is too weak to develop stratiform clouds at higher heights. The weaker front-to-rear flow then creates stratiform clouds at lower levels, producing excessive precipitation at the trailing region. The vertical velocity spectra also provide further evidence that the increased small-scale spurious convections disrupt the large-scale coherent updrafts (e.g., front-to-rear flow). Compared to simulations with numerical dissipation, the no-dissipation simulation has shown less resolved energy at larger scales (including the energy-containing scale) but more energy at small scales close to Nyquist limits (Fig. 6c). In addition, the λ_p of the no-dissipation simulation is at around 2 km, which is smaller than that in simulations with dissipation. This decrease of λ_p is consistent with the more spurious small-scale convections seen in Fig. 7a.

c. 1-km resolution simulations

The 200-m and 4-km simulations represent two extremes. The numerical dissipation acts more on physically realistic convective cells in the 4-km simulation, while it acts more on numerical spurious oscillations in 200-m simulations. At the 1-km simulations, although convective cells are partly dampened, the role of numerical dissipation in dampening unphysical numerical oscillations is indispensable.

The 1-km simulation has shown similar results to the 200-m simulation. The no-dissipation simulation shows underestimated convective updrafts in the convective region while underdeveloped high-level trailing stratiform cloud (Figs. 10a, f). In contrast, the cases with non-zero artificial dissipation have shown stronger convective updrafts, precipitation in the convective region and well-developed high-level clouds in the stratiform region (Figs. 10g, h, i, j). The 1-km simulations are also investigated using the tracer method. Similar to 200-m simulations, the excessive entrainment and mixing from spurious numerical oscillations are probably the cause of weaker convective updrafts.

Different from the 200-m simulations, the dominant convective cells in 1-km simulations are partly dampened. The partly dampened signal can be seen from the energy spectra (Fig. 6b). The λ_p in the 1-km simulations varies considerably with the degree of numerical dissipation. The increased numerical dissipation increases the cell sizes, subsequently increasing the λ_p. In the

200-m simulations, the damping acts primarily on numerical oscillations. Increasing the degree of numerical dissipation only increases the spectral slope below $6\Delta x$ (Fig. 6c). Although physical convective cells are dampened at both the 1-km and 4-km simulations, we stress that they are two different patterns. The energy spectra of the 1-km simulations resemble that of the 200-m simulations more (Figs. 5b, c). Compared with simulations with numerical dissipation, the no-dissipation simulations show weaker energy at large scales but stronger energy at small scales, indicating the increased small scale spurious convections weaken the large scale convective flow (Fig. 6b). However, in the 4-km simulations, the no-dissipation case shows overall larger energy across all scales than the simulations with numerical dissipation (Fig. 6a).

6. The Dynamic Reconstruction Method

The numerical dissipation, which arises from truncation errors in grid discretization, can greatly impact the squall line structure and precipitation distribution. Compared to traditional LES closures, the DRM allows turbulence backscatter and reduces the numerical errors from grid discretization (Gullbrand and Chow 2003). Therefore, how the physical mixing from DRM interacts with numerical dissipation from the advection scheme is worthy of further exploration. This section evaluates the performance of DRM in two gray zone resolutions with WENO5 and ODD5 advection schemes.

a. 4-km resolution simulations

1) Combination with fifth-order WENO scheme

The combination of the WENO5 advection scheme with traditional TKE (WENO5+TKE) has shown significant underestimations of convective precipitation and overestimations of stratiform precipitation in the 4-km simulations because the numerical dissipation from the WENO5 scheme dampens physical convective cells significantly. The use of DRM2 or DRM0, in replacement of TKE, can significantly reduce the numerical dissipation effects on convective cells and enhance dominant convective updrafts (Supplementary Figs. S3,4). The DRM2, in particular, improves the precipitation distribution in terms of increasing the underestimated convective precipitation, reducing the excessive stratiform precipitation, and simulating the peak precipitation location relative to the cold pool edge (Fig. 11a). The DRM0 shows unsatisfying results in which the

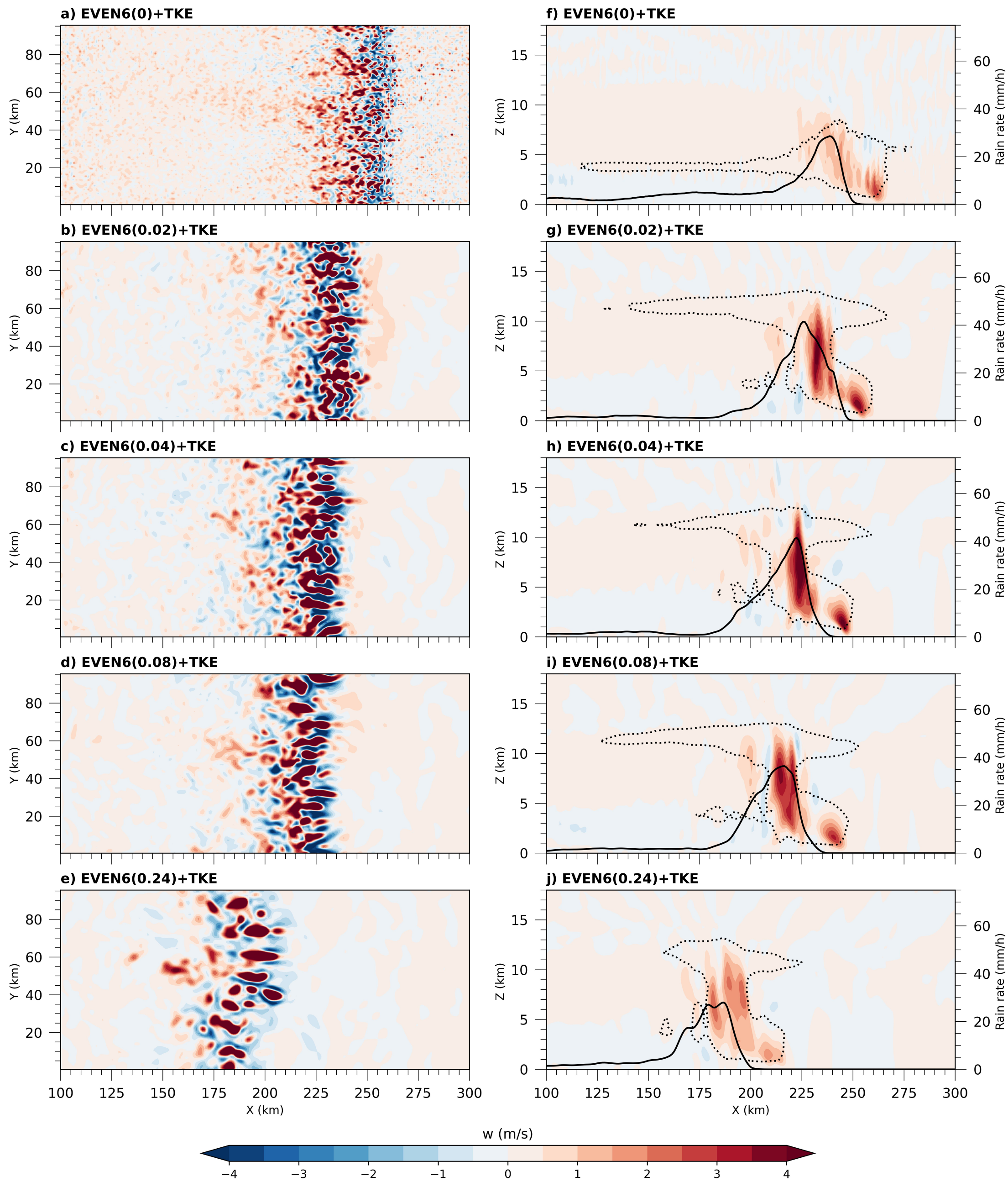

Fig. 10. Same as Fig. 5 except using 1-km resolution.

convective precipitation is severely underestimated (Fig. 11a). However, there are still signs of improvement in the location of peak precipitation. The DRM0 shifts the convective precipitation peak to a location that is closer to the gust front, which is in better agreement with the benchmark simulation (Fig. 11a).

The better performance of DRM can be seen from the vertical velocity spectra (Fig. 12a). The DRMs (DRM0 and DRM2) show more resolved energy than the TKE scheme. This is probably because the backscatter of SFS in DRM allows more resolved energy, less imposed numerical dissipation on convective cells and stronger convective updrafts. In the along-squall-line direction, DRM2 resolves more energy at large scales than DRM0 (Fig. 12a). The resolved energy of DRM2 is slightly overestimated but in closer agreement with the benchmark simulation spectrum at large scales. At smaller scales, the DRM2 shows a decreasing energy trend with smaller wavelengths, suggesting that small-scale energy is dissipated. DRM0, in contrast, shows an increasing energy trend with smaller wavelengths. The small-scale motions are not well dissipated in DRM0. The better performance of DRM2 compared to DRM0 is probably because the higher order reconstruction of RSFS allows more energy to be backscattered from SFS to resolved scales. This backscatter reduces the effects of excessive numerical dissipation from the WENO5 scheme.

The precipitation distribution of the DRM2+WENO5 combination is very similar to that of the EVEN6(0)+TKE (Fig. 11a). These two combinations represent two different pathways to reduce of effects of excessive numerical dissipation in the WENO5+TKE combination, with one changing the turbulence scheme (by replacing the TKE with DRMs), and another changing the advections schemes (by replacing the WENO5 with EVEN6). The vertical velocity spectra of the two combinations also show a great consistency for scales larger than 24 km (λ_d) (Fig. 6a). However, at scales smaller than λ_d, the WENO5+DRM2 shows energy decay, while the energy of no-dissipation case EVEN6(0)+TKE continues to increase (Fig. 12a). This energy accumulation at the small wavelengths may cause instabilities. Therefore, the advantage of using the turbulence scheme (WENO5+DRM2) over the no-dissipation advection scheme EVEN6(0)+TKE is that the former combination is more stable. Studies have shown that in real case simulations where the atmospheric conditions are more random temporally and spatially, centered order advection schemes without artificial numerical dissipation often lead to spurious grid scale erroneous convections (e.g., Kusaka et al. 2005).

2) Combination with fifth-order scheme

The DRMs are also combined with the ODD5 advection scheme. The OOD5 scheme has shown less numerical dissipation than the WENO5 scheme, and the convective precipitation is much

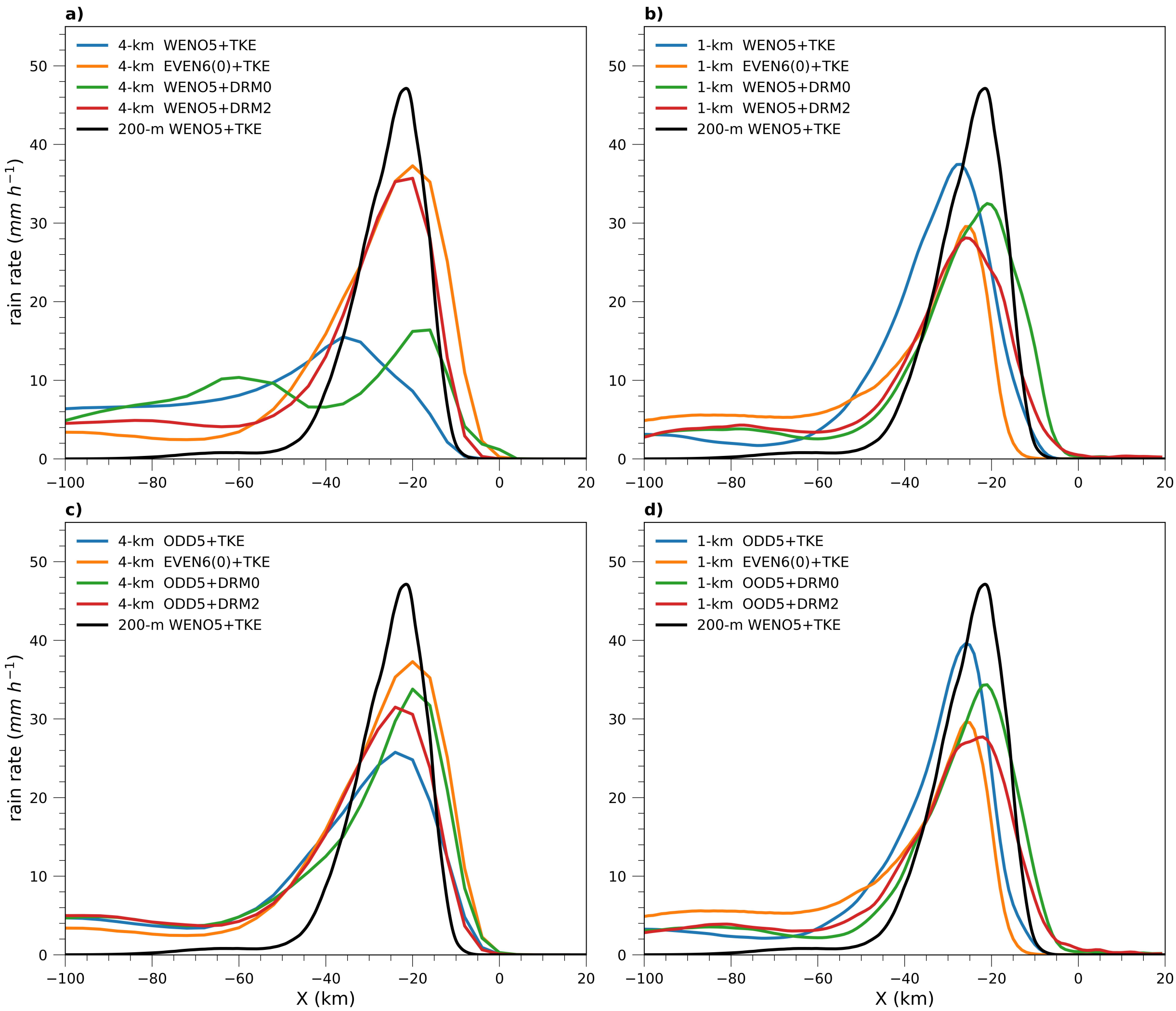

FIG. 11. The along squall line averaged steady-state rain rate distribution. Same to Fig. 3, but shows results: a) 4-km resolution simulations using the WENO5 as the advection scheme, and the DRM0, DRM2 as the turbulence model, b) 1-km resolution simulation using the WENO5 as the advection scheme, and DRM0, DRM2 as the turbulence model, c) 4-km resolution simulations using the WENO5 as the advection scheme, and the DRM0, DRM2 as the turbulence model, d) 1-km resolution simulations using the ODD5 as the advection scheme, and the DRM0, DRM2 as the turbulence model. For easy comparison in single plots, the simulations previously shown in Fig. 3 are also included

stronger in the 4-km simulations (Fig. 11c). Both DRM2 and DRM0 have shown improvement in increasing convective precipitation (Fig. 11c). However, the DRM0 shows slightly stronger convective precipitation and resolved energy than the DRM2 (Figs. 11c, 12c). This suggests that for the ODD5, where the numerical dissipation is relatively less, the DRM0 may be more appropriate. The DRM0 has a lower-order reconstruction of RSFS and allows less energy backscatter. Therefore, the equivalent effect in reducing the numerical dissipation from the advection scheme is less. In summary, the DRM0 is more appropriate for the ODD5 scheme, while the high-order DRM2 is more appropriately used for a more dissipative WENO5 scheme. These results imply that the optimal combination of the advection scheme and the order of DRM warrants further investigation.

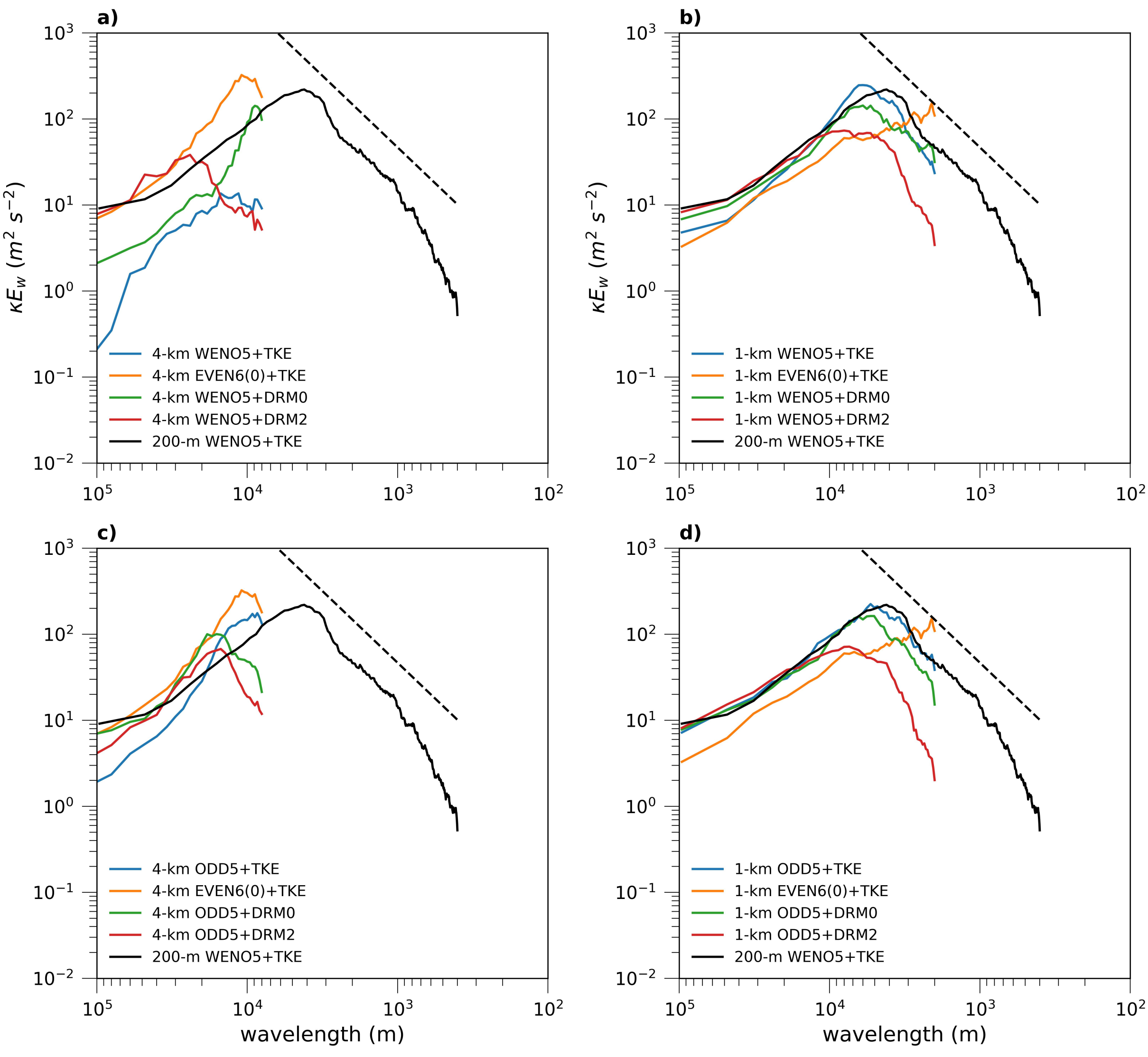

FIG. 12. One-dimensional vertical velocity (along squall line direction, at 5 km above the surface) spectra of simulations with horizontal grid resolutions of 1 km and 4 km. a) The spectra of 4-km simulations of WENO5+TKE, EVEN6(0)+TKE, WENO5+DRM0, and WENO5+DRM2. b) same as a) expect shows 1 km simulations. c) The spectra of 4-km simulations of ODD5+TKE, EVEN6(0)+TKE, ODD5+DRM0, and ODD5+DRM2. d) same as c) expect shows 1 km simulations. The spectrum of the 200 m benchmark simulation is plotted for reference. The black dashed line indicates a $k^{-\frac{5}{3}}$ spectrum.

b. 1-km resolution simulations

Based on previous discussions in section 5, the numerical dissipation from the advection schemes is indispensable in the 1-km simulations. Otherwise, spurious numerical oscillations are generated and weaken the convective updrafts by increasing the entrainments. On the contrary to 4-km simulations, both DRM0 and DRM2 show worse performance in simulating the squall line precipitation distribution than the traditional TKE model regardless of its combination with WENO5 or ODD5 advection scheme (Figs. 11b, d). The convective precipitation in DRMs is underestimated, while the stratiform precipitation is overestimated (Figs. 11b, d). In addition, the high-order DRM2 shows weaker convective precipitation than DRM0 and resembles the precipitation distribution with the EVEN6(0)+TKE combination. These deteriorated performances stem from the increased occurrence of spurious convections in DRM simulations.

The increased small-scale convections with DRM0 and DRM2 schemes are further illustrated by the instantaneous vertical velocity field (Figs. 13b, c). Compared to the WENO5+TKE, the combinations of WENO5 with DRMs show increased spurious oscillations ahead of squall lines (Figs. 13). These spurious oscillations are not seen for 4-km resolution WENO5+DRM2 or WENO5+DRM0 simulations (Supplementary Fig. S4). The WENO5+DRM2 has a higher degree of spurious oscillations than the WENO5+DRM0 (Figs. 13). The more spurious fields weaken the convective updrafts more. The vertical velocity spectra (Figs. 12b, d) also convey the message that the backscattering DRMs weaken the dominant convective updrafts. The spectra peak which indicates the intensities of energy-containing turbulences is smaller in WENO5+DRM2(ODD5+DRM2) than that in WENO5+TKE(ODD5+TKE). The WENO5+DRM2 (ODD5+DRM2) has shown an even weaker spectra peak than the WENO5+DRM0 (ODD5+DRM0). It is also interesting to note that the convective cells of DRM2+WENO5 or DRM0+WENO5 simulations are not in a grid scale (Figs. 13c, d). Although the oscillations from the DRM2+WENO5 and DRM0+WENO5 simulations are similar to the pattern seen in EVEN6(0)+TKE (Figs. 13b, c, d), they are indeed different because the oscillations are mostly from the numerical errors in the EVEN6(0)+TKE, while the oscillations are mostly from the physical backscatter of small-scale energy in the DRM simulations.

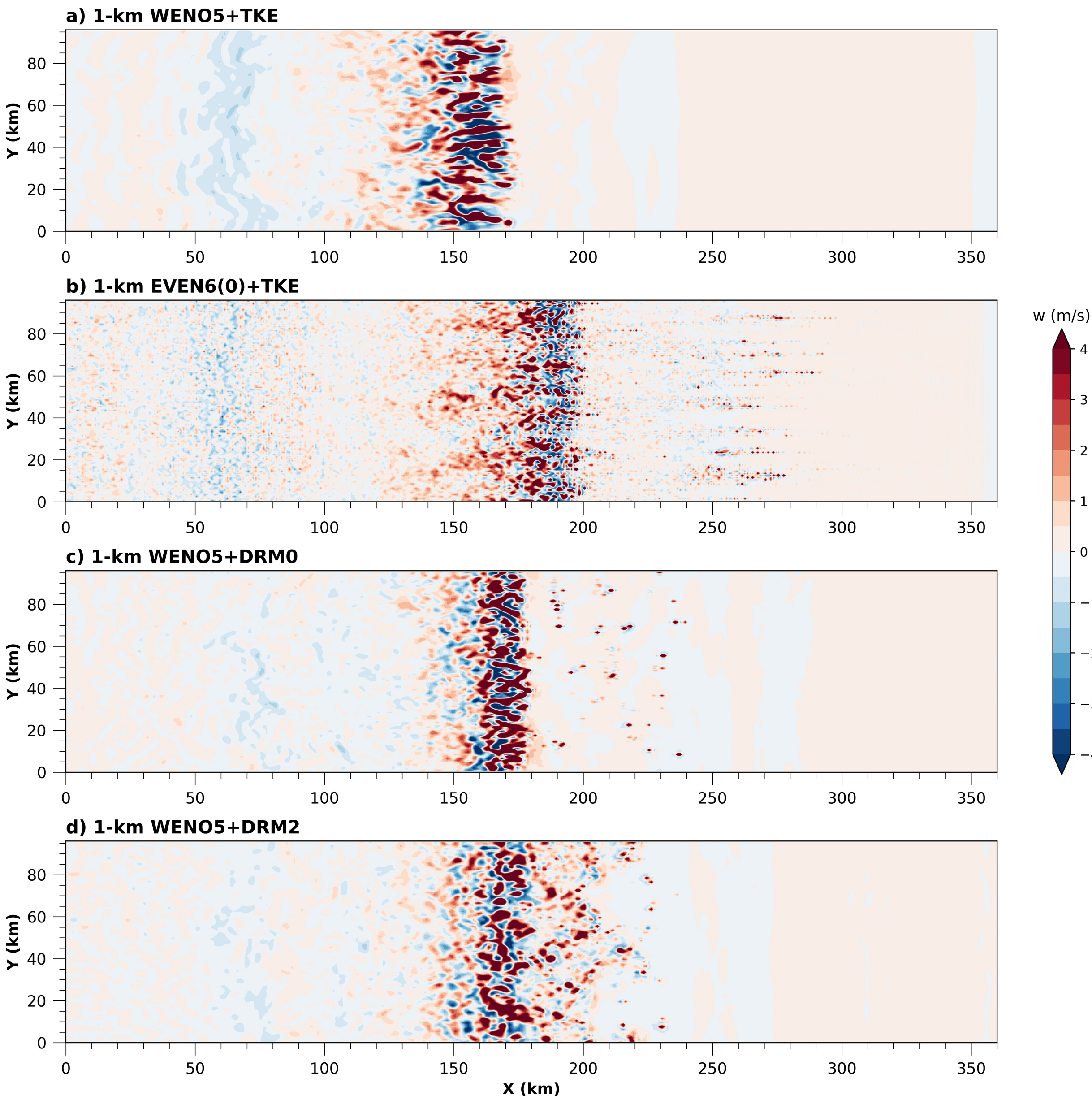

FIG. 13. The vertical velocity of a horizontal plane at a height of 5 km in the 4th hour for 1-km resolution simulations a)1-km WENO5+TKE, b) 1-km EVEN6(0)+TKE, c) 1-km WENO5+DRM0, d) 1-km WENO5+DRM2

7. Conclusions

In this study, we evaluated three numerical advection schemes and investigated the impact of numerical dissipation on squall line simulations with various grid resolutions (200 m, 1 km, and 4 km). For squall line simulations, the 200 m grid size falls into the LES resolution range, while 1 km and 4 km grid sizes are at gray zone resolutions.

The role of numerical dissipation are different at different grid resolutions. At the LES resolution, numerical dissipation is necessary, because without it, spurious numerical oscillations may develop into numerous small-scale convective cells. These cells increase the mixing and entrainment, further preventing the formation of strong and coherent updrafts. These weaker updrafts lead to much weaker convective precipitation and front-to-rear flow, which forms trailing clouds at lower levels, producing excessive stratiform precipitation. The needed dissipation can be provided by the implicit dissipation of odd-order schemes or by adding artificial numerical dissipation to the even-order schemes. The simulation results are not sensitive to the strength of numerical dissipation at the LES resolution, because the numerical dissipation acts primarily on turbulent eddies that are far smaller than the dominant physical convective cells.

In the gray zone resolution of 4 km, the numerical dissipation dampens physical convective cells significantly, and convective updrafts are generally weak. The weaker front-to-rear flows, similarly, produce excessive stratiform precipitation but less convective precipitation. Therefore, advection schemes with minimum numerical dissipation are recommended. In the gray zone resolution of 1 km, although convective cells are also dampened, the numerical dissipation in the advection scheme is still important. Without sufficient numerical dissipation, sporadic convections generated from spurious numerical oscillations increase mixing and weaken the front-to-rear flow.

The dynamic reconstruction model (DRM) is an advanced turbulence closure model that can model both forward- and backscatter of SGS turbulence (Chow et al. 2005), potentially reducing the numerical dissipation effects in advection schemes. In combination with two advection schemes that have implicit numerical dissipation, the DRM is evaluated at two gray zone resolutions (1 and 4 km). In the gray zone resolution of 4 km, the application of DRM can effectively improve the squall structures and the corresponding precipitation distributions by reducing the overpredicted stratiform precipitation and increasing the underpredicted convective precipitation. The numerical dissipation at the 4-km resolution is excessive and undesired for its effect on dampening physical convective updrafts. The ability to model backscatter turbulence in DRM allows numerical dissipation effects to be reduced, enhances convective updrafts and therefore improves the squall line simulations. In addition, the combination between advections scheme and DRMs is also important. High-order (low-order) DRM should be combined with advection schemes that have stronger (weaker) numerical dissipation. Two versions of DRM, DRM0 and

DRM2, are evaluated. DRM2 has stronger turbulence backscatter effects than DRM0. When combined with a more dissipative advetion scheme (WENO5), DRM2 excels greatly than DRM0. When combined with a less dissipative advection scheme (OOD5), the DRM0 excels than DRM2.

In the gray zone resolution of 1 km, the application of DRM cannot effectively improve squall line precipitation distribution and lead to spurious oscillations. The numerical dissipation effect at the 1-km resolution is desired for the suppression of numerical oscillations. The backscatter from DRM has the effect of reducing numerical dissipation effects and leads to excessive generation of small-scale convective motions. The 1-km simulations are sensitive to the reduction of numerical dissipation effects probably because the grid scale numerical oscillations are close to the sizes of individual convective cores, which are around 1 km (LeMone and Zipser 1980; Shi et al. 2019), and thereby can easily develop into spurious convection in the unstable environment. Thus, the DRMs cannot improve squall line simulations regardless of their combinations with less or more disspiative numerical advection scheme. Of note, in the LES resolution of 200 m, the application of DRM does not cause spurious convection although numerical dissipation from the advection scheme is indispensable. This is because the turbulence backscatter in LES is not as important as that in gray zone simulations (Chow et al. 2019).

This work reveals that numerical dissipation effects vary across different gray zone resolutions in a squall line simulation. The numerical dissipation is excessive and undesired at certain gray zone resolutions, but essential at other gray zone resolutions. The DRM turbulence model assumes subfilter-scale effects include backscatter and reconstructs such effects based on resolved flows. It can improve the squall line simulation at gray resolutions where numerical dissipation acts more on convective cells than numerical oscillations, but it may lead to spurious oscillations at gray zone resolutions when the numerical dissipation effect is indeed indispensable for dampening numerical oscillations, which, in DRM, can lead to spurious backscatter.

Acknowledgments. The work is substantially supported by a grant from the Research Grants Council (RGC) of the Hong Kong Special Administrative Region, China (Project Reference Number: AoE/P-601/23-N) and the Center for Ocean Research in Hong Kong and Macau (CORE), a joint research center between the Laoshan Laboratory and the Hong Kong University of Science and Technology (HKUST). JC is additionally supported by RGC grant AoE/E-603/18 and HKUST-16301721. The authors thank HKUST Fok Ying Tung Research Institute and National Supercomputing Center in Guangzhou Nansha sub-center for providing high-performance computational resources.

References

Arakawa, A., and V. R. Lamb, 1977: Computational design of the basic dynamical processes of the UCLA general circulation model. *General circulation models of the atmosphere*, **17 (Supplement C)**, 173–265.

Beare, R. J., 2014: A Length Scale Defining Partially-Resolved Boundary-Layer Turbulence Simulations. *Boundary-Layer Meteorology*, **151 (1)**, 39–55, https://doi.org/10.1007/s10546-013-9881-3.

Borges, R., M. Carmona, B. Costa, and W. S. Don, 2008: An improved weighted essentially non-oscillatory scheme for hyperbolic conservation laws. *Journal of computational physics*, **227 (6)**, 3191–3211.

Bryan, G. H., 2005: Spurious Convective Organization in Simulated Squall Lines Owing to Moist Absolutely Unstable Layers. *Monthly Weather Review*, **133 (7)**, 1978–1997, https://doi.org/10.1175/MWR2952.1.

Bryan, G. H., 2012: Effects of Surface Exchange Coefficients and Turbulence Length Scales on the Intensity and Structure of Numerically Simulated Hurricanes. *Monthly Weather Review*, **140 (4)**, 1125–1143, https://doi.org/10.1175/MWR-D-11-00231.1.

Bryan, G. H., and J. M. Fritsch, 2002: A Benchmark Simulation for Moist Nonhydrostatic Numerical Models. *Monthly Weather Review*, **130 (12)**, 2917–2928, https://doi.org/10.1175/1520-0493(2002)130⟨2917:ABSFMN⟩2.0.CO;2.

Bryan, G. H., J. C. Knievel, and M. D. Parker, 2006: A Multimodel Assessment of RKW Theory's Relevance to Squall-Line Characteristics. *Monthly Weather Review*, **134 (10)**, 2772–2792, https://doi.org/10.1175/MWR3226.1.

Bryan, G. H., and H. Morrison, 2012: Sensitivity of a Simulated Squall Line to Horizontal Resolution and Parameterization of Microphysics. *Monthly Weather Review*, **140 (1)**, 202–225, https://doi.org/10.1175/MWR-D-11-00046.1.

Bryan, G. H., J. C. Wyngaard, and J. M. Fritsch, 2003: Resolution Requirements for the Simulation of Deep Moist Convection. *Monthly Weather Review*, **131 (10)**, 2394–2416, https://doi.org/10.1175/1520-0493(2003)131⟨2394:RRFTSO⟩2.0.CO;2.

Chow, F., C. Schär, N. Ban, K. Lundquist, L. Schlemmer, and X. Shi, 2019: Crossing Multiple Gray Zones in the Transition from Mesoscale to Microscale Simulation over Complex Terrain. *Atmosphere*, **10 (5)**, 274, https://doi.org/10.3390/atmos10050274.

Chow, F. K., R. L. Street, M. Xue, and J. H. Ferziger, 2005: Explicit Filtering and Reconstruction Turbulence Modeling for Large-Eddy Simulation of Neutral Boundary Layer Flow. *Journal of the Atmospheric Sciences*, **62 (7)**, 2058–2077, https://doi.org/10.1175/JAS3456.1.

Deardorff, J. W., 1980: Stratocumulus-capped mixed layers derived from a three-dimensional model. *Boundary-Layer Meteorology*, **18 (4)**, 495–527, https://doi.org/10.1007/BF00119502.

Durran, D. R., 2010: *Numerical methods for fluid dynamics: With applications to geophysics*, Vol. 32. Springer Science & Business Media.

Gullbrand, J., and F. K. Chow, 2003: The effect of numerical errors and turbulence models in large-eddy simulations of channel flow, with and without explicit filtering. *Journal of Fluid Mechanics*, **495**, 323–341, https://doi.org/10.1017/S0022112003006268.

Honnert, R., and Coauthors, 2020: The Atmospheric Boundary Layer and the "Gray Zone" of Turbulence: A Critical Review. *Journal of Geophysical Research: Atmospheres*, **125 (13)**, https://doi.org/10.1029/2019JD030317.

Jiang, G.-S., and C.-W. Shu, 1996: Efficient implementation of weighted ENO schemes. *Journal of computational physics*, **126 (1)**, 202–228.

Knievel, J. C., G. H. Bryan, and J. P. Hacker, 2007: Explicit Numerical Diffusion in the WRF Model. *Monthly Weather Review*, **135 (11)**, 3808–3824, https://doi.org/10.1175/2007MWR2100.1.

Kusaka, H., A. Crook, J. C. Knievel, and J. Dudhia, 2005: Sensitivity of the WRF Model to Advection and Diffusion Schemes for Simulation of Heavy Rainfall along the Baiu Front. *SOLA*, **1**, 177–180, https://doi.org/10.2151/sola.2005-046.

Lai, K. T., and M. L. Waite, 2020: Resolution Dependence and Subfilter-Scale Motions in Idealized Squall-Line Simulations. *Monthly Weather Review*, **148 (7)**, 3059–3078, https://doi.org/10.1175/MWR-D-19-0330.1.

LeMone, M. A., and E. J. Zipser, 1980: Cumulonimbus vertical velocity events in gate. part i: Diameter, intensity and mass flux. *Journal of the Atmospheric Sciences*, **37 (11)**, 2444–2457.

Moeng, C.-H., 1984: A large-eddy-simulation model for the study of planetary boundary-layer turbulence. *Journal of the Atmospheric Sciences*, **41 (13)**, 2052–2062.

Morrison, H., G. Thompson, and V. Tatarskii, 2009: Impact of Cloud Microphysics on the Development of Trailing Stratiform Precipitation in a Simulated Squall Line: Comparison of One- and Two-Moment Schemes. *Monthly Weather Review*, **137 (3)**, 991–1007, https://doi.org/10.1175/2008MWR2556.1.

Parodi, A., and S. Tanelli, 2010: Influence of turbulence parameterizations on high-resolution numerical modeling of tropical convection observed during the TC4 field campaign. *Journal of Geophysical Research: Atmospheres*, **115 (D10)**, https://doi.org/https://doi.org/10.1029/2009JD013302.

Pressel, K. G., C. M. Kaul, T. Schneider, Z. Tan, and S. Mishra, 2015: Large-eddy simulation in an anelastic framework with closed water and entropy balances. *Journal of Advances in Modeling Earth Systems*, **7 (3)**, 1425–1456, https://doi.org/10.1002/2015MS000496.

Shi, X., F. K. Chow, R. L. Street, and G. H. Bryan, 2018a: An Evaluation of LES Turbulence Models for Scalar Mixing in the Stratocumulus-Capped Boundary Layer. *Journal of the Atmospheric Sciences*, **75 (5)**, 1499–1507, https://doi.org/10.1175/JAS-D-17-0392.1.

Shi, X., F. K. Chow, R. L. Street, and G. H. Bryan, 2019: Key Elements of Turbulence Closures for Simulating Deep Convection at Kilometer-Scale Resolution. *Journal of Advances in Modeling Earth Systems*, **11 (3)**, 818–838, https://doi.org/10.1029/2018MS001446.

Shi, X., H. L. Hagen, F. K. Chow, G. H. Bryan, and R. L. Street, 2018b: Large-Eddy Simulation of the Stratocumulus-Capped Boundary Layer with Explicit Filtering and Reconstruction Turbulence Modeling. *Journal of the Atmospheric Sciences*, **75 (2)**, 611–637, https://doi.org/10.1175/JAS-D-17-0162.1.

Shin, H. H., and S.-Y. Hong, 2015: Representation of the Subgrid-Scale Turbulent Transport in Convective Boundary Layers at Gray-Zone Resolutions. *Monthly Weather Review*, **143 (1)**, 250–271, https://doi.org/10.1175/MWR-D-14-00116.1.

Simon, J. S., B. Zhou, J. D. Mirocha, and F. K. Chow, 2019: Explicit Filtering and Reconstruction to Reduce Grid Dependence in Convective Boundary Layer Simulations Using WRF-LES. *Monthly Weather Review*, **147 (5)**, 1805–1821, https://doi.org/10.1175/MWR-D-18-0205.1.

Skamarock, W. C., 2004: Evaluating Mesoscale NWP Models Using Kinetic Energy Spectra. *Monthly Weather Review*, **132 (12)**, 3019–3032, https://doi.org/10.1175/MWR2830.1.

Skamarock, W. C., and Coauthors, 2008: A description of the advanced research WRF version 3. *NCAR technical note*, **475**, 113.

Stolz, S., and N. A. Adams, 1999: An approximate deconvolution procedure for large-eddy simulation. *Physics of Fluids*, **11 (7)**, 1699–1701.

Sun, S., B. Zhou, M. Xue, and K. Zhu, 2021: Scale-Similarity Subgrid-Scale Turbulence Closure for Supercell Simulations at Kilometer-Scale Resolutions: Comparison against a Large-Eddy Simulation. *Journal of the Atmospheric Sciences*, **78 (2)**, 417–437, https://doi.org/10.1175/JAS-D-20-0187.1.

Takemi, T., and R. Rotunno, 2003: The Effects of Subgrid Model Mixing and Numerical Filtering in Simulations of Mesoscale Cloud Systems. *Monthly Weather Review*, **131 (9)**, 2085–2101, https://doi.org/10.1175/1520-0493(2003)131⟨2085:TEOSMM⟩2.0.CO;2.

Wang, A., Y. Pan, and P. M. Markowski, 2021: The Influence of WENO Schemes on Large-Eddy Simulations of a Neutral Atmospheric Boundary Layer. *Journal of the Atmospheric Sciences*, https://doi.org/10.1175/JAS-D-21-0033.1.

Weisman, M. L., and R. Rotunno, 2004: “A Theory for Strong Long-Lived Squall Lines” Revisited. *Journal of the Atmospheric Sciences*, **61 (4)**, 361–382, https://doi.org/10.1175/1520-0469(2004)061⟨0361:ATFSLS⟩2.0.CO;2.

Weisman, M. L., W. C. Skamarock, and J. B. Klemp, 1997: The Resolution Dependence of Explicitly Modeled Convective Systems. *Monthly Weather Review*, **125 (4)**, 527–548, https://doi.org/10.1175/1520-0493(1997)125⟨0527:TRDOEM⟩2.0.CO;2.

Wicker, L. J., and W. C. Skamarock, 2002: Time-splitting methods for elastic models using forward time schemes. *Monthly weather review*, **130 (8)**, 2088–2097.

Wong, V., and D. K. Lilly, 1994: A comparison of two dynamic subgrid closure methods for turbulent thermal convection. *Physics of Fluids*, **6 (2)**, 1016–1023.

Xue, M., 2000: High-Order Monotonic Numerical Diffusion and Smoothing. *Monthly weather review*, **128 (8)**, 2853–2864.